



POCATOM



STATE ATOMIC ENERGY CORPORATION "ROSATOM"

**ZIRCONIUM, INDUSTRIAL ZIRCONIUM ALLOYS Zr-1%Nb and Zr-2.5%Nb:
 $\alpha \rightarrow \omega$ TRANSITION,
TEMPERATURE DEPENDENCES OF DYNAMIC BEHAVIOR, DEFORMATION AND
SPALLATION MECHANISMS**

Alexander V. Pavlenko,

S.N. Malyugina, D.N. Kazakov, S.S. Mokrushin, A.S. Mayorova, O.E. Kozelkov, A.V. Dobromyslov, N.I. Taluts, S.Yu. Filatov, A.E. Shestakov, A.M. Sedov

Russian Federal Nuclear Center – Zababakhin All-Russia Research Institute of Technical Physics (RFNC-VNIITF), Snezhinsk, Russia

Supported by ROSATOM

State Contract No. H.4x.44.90.13.1111

State Contract No. H.4x.44.9Б.16.1012

Shock-wave investigations – **RFNC-VNIITF:**

S.N. Malyugina, D.N. Kazakov, S.S. Mokrushin,
A.S. Mayorova, O.E. Kozelkov, S.Yu. Filatov

Material science investigations were performed at:

RFNC-VNIITF by

A.E. Shestakov, A.V. Sedov and

Metal Physics Institute, RAS Ural Branch by

A.V. Dobromyslov and N.I. Taluts

Problem statement and useful discussions – G.I. Kanel

(Deputy Director of JIHT RAS, Institute of Problems of Chemical
Physics)

The work was supported by Rosatom under State Contracts
No. H.4x.44.90.13.1111 and H.4x.44.9Б.16.1012

Zirconium

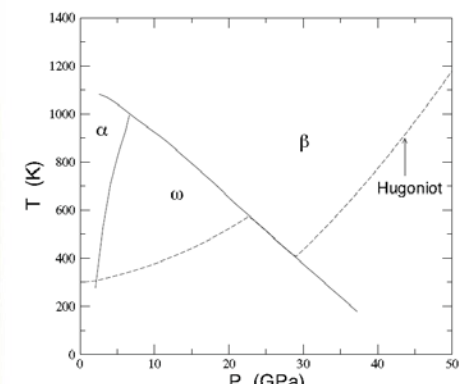
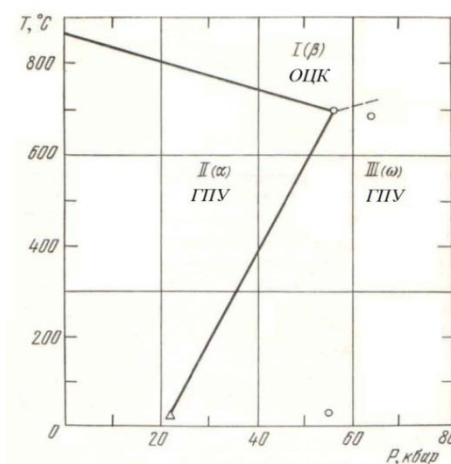
Zirconium – is a polymorphous metal. Its low-temperature modification α (α -zirconium) exists at the temperature up to 862°C and has HCP crystalline lattice (α -phase).

High-temperature modification β (β -zirconium) has BCC crystalline lattice. Transition ($\alpha \leftrightarrow \beta$) is of non-diffusion martensitic nature.



Metastable ω -phase can form along with the polymorphic transition ($\alpha \leftrightarrow \beta$) at the pressure higher than 6 GPa.

Фаза	Кристалл. структура	Параметры решетки, нм	ρ , г/см ³	Условия существования
α	ГПУ	$a=0,323118$ $c=0,514634$ $c/a=1,59271$	6,51 6,49	$T \leq 862^{\circ}\text{C}$
β	ОЦК	$a=0,359$	6,54 6,4	$T = 862-1855^{\circ}\text{C}$
ω	ГПУ	$a=0,5036$ $c=0,3109$ $c/a=0,61736$	6,68	$P > 6 \text{ ГПа}$



Calculated zirconium Hugoniot and phase diagram.

Studying Dynamic Behavior of Zirconium



- **G.C. Kaschner, G.T. Gray III, and S.R. Chen.**

The Influence of Texture and Impurities On The Mechanical Behavior of Zirconium. In Proc. Shock Compression of Condensed Matter – 1997.

- **G.T. Gray III, N.K. Bourne, M .A . Zocher, P.J. Maudlin, and J.C.F. Millett.**

Influence of Crystallographic Anisotropy On The Hopkinson Fracture “Spallation” of Zirconium. In Proc. Shock Compression of Condensed Matter – 1999.

- **E. Cerreta, G.T. Gray III, B.L. Henrie, D.W. Brown, R.S. Hixson and P.A. Rigg.**

The Influence of Peak Stress on the Mechanical Behavior and the Substructural Evolution in Shockprestrained Zirconium. In Proc. Shock Compression of Condensed Matter – 2003

- **E. Cerreta, G.T. Gray III, A.C. Lawson, C.E. Morris, R.S. Hixson, and P.A. Rigg.**

The Influence of Interstitial Oxygen On The Alpha To Omega Phase Transition In Titanium And Zirconium. In Proc. Shock Compression of Condensed Matter – 2005.

- **P.A. Rigg, C.W. Greeff, M.D. Knudson and G.T. Gray, III.**

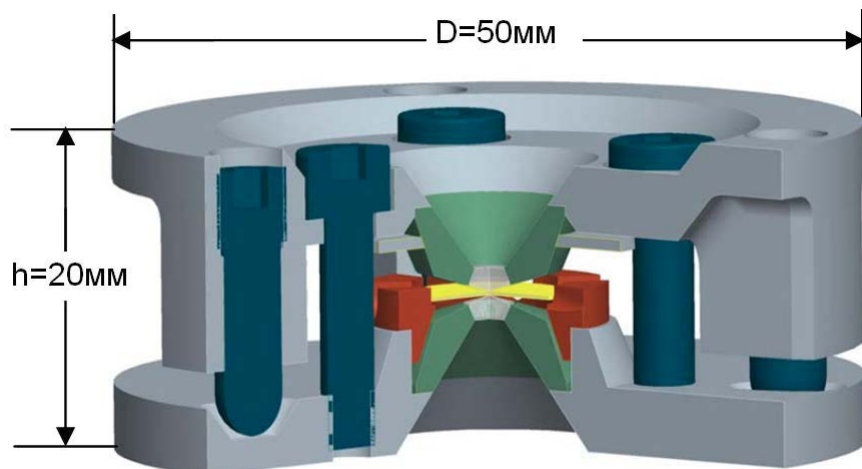
Influence of Impurities On The Solid-Solid Phase Transitions In Zirconium. In Proc. Shock Compression of Condensed Matter – 2009.

Experimental setup

One-stage gas guns of the 44-mm caliber



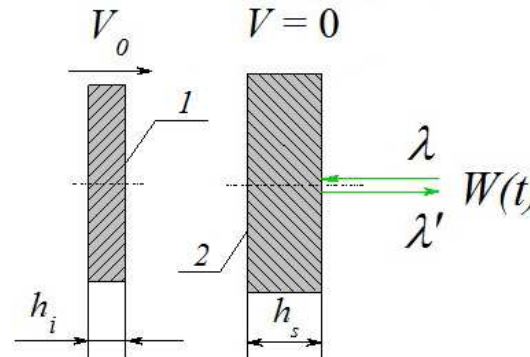
0.05...1 km/s and 0.5...2.5 km/s



Diamond anvils - Boehler-Almax cells.

Radiation – MoK α $\lambda = 0.711 \text{ \AA}$. Transmitting medium – NaCl. ($\Delta P = \pm 0.3 \text{ GPa}$)

Experimental setup



Registration

$W(t)$ - 1.4.. 0.5 % (1.4.. 2.2 ns) // VISAR

$W(t)$ - 1.2.. 0.7 % (2..4 ns) // PDV

Impactor velocity V_0 - 0.2 % //pins

Structure - Neophot-21 light microscope,
Microstructure, phase, and composition of elements in
Quanta-200 scanning electron microscope; JEM-200CX
transmission electron microscope;
X-ray diffraction analysis DRON3 (CuK α);
Microhardness - PMT-3 under 50 g loading.

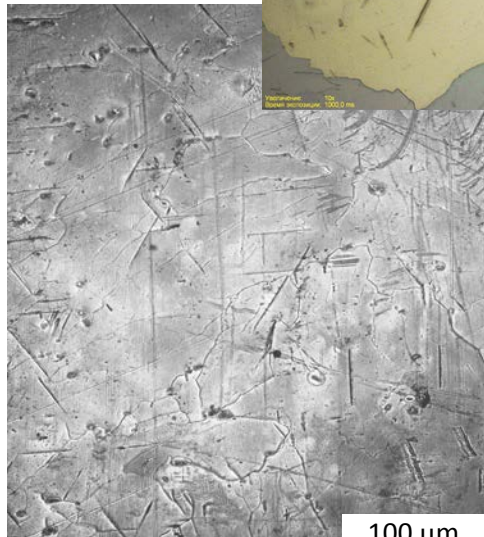
Initial Structure of Pure Zirconium Samples



Impurities – O, Fe ~ 470 ppm

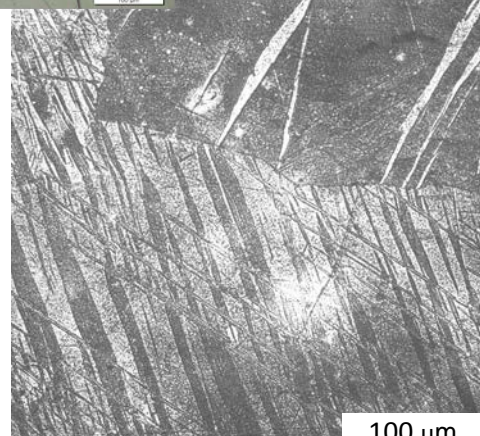
X-ray diffraction patterns show only peaks of close-packed hexagonal α -phase

Coarse-grained



Grain size – 3...7 mm

Presence of macro-twins

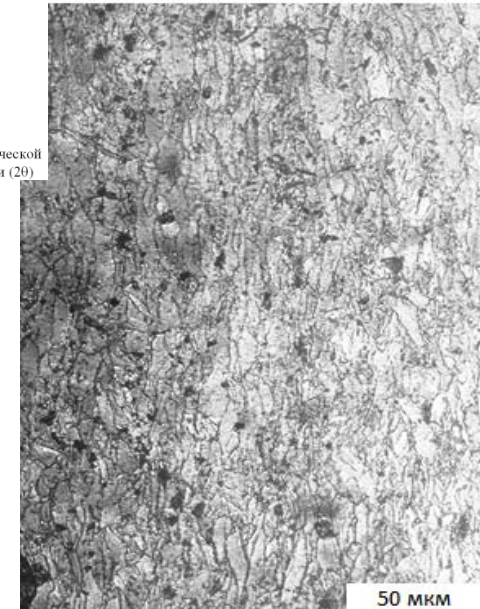


100 μm

100 μm

100 μm

Thermomechanical treatment



Grain size – 12..25 μm
 $H_{\mu} = 1097 \pm 40 \text{ MPa}$

50 μm

Initial Structure of Pure Zirconium Samples



Impurities—O, Fe ~ 470 ppm
Coarse-grained 3..7 mm

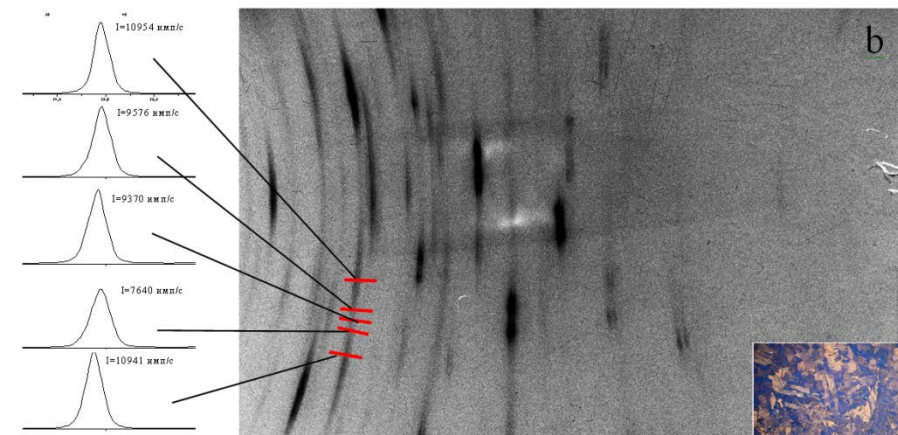
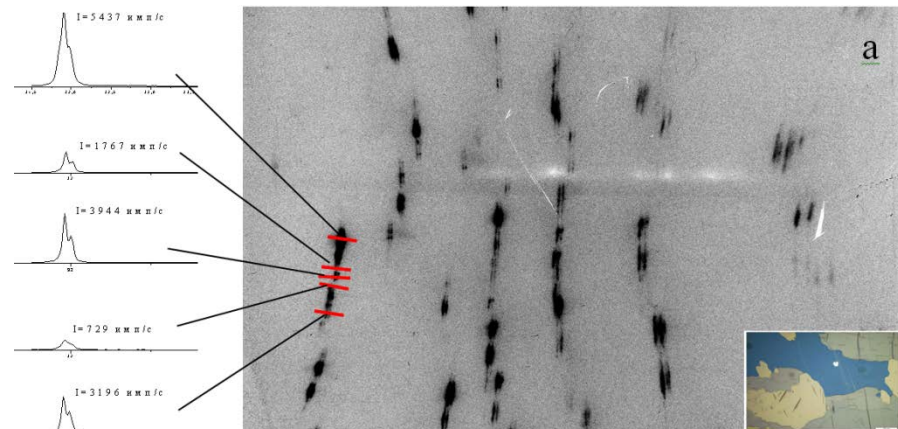


Thermomechanical treatment



Grain size – 12..25 μm

X-ray diffraction patterns show only peaks of close-packed hexagonal α -phase



Zirconium Alloy E100



Composition:

- Basic metal – Zirconium ($_{40}\text{Zr}$)
- Impurities (O ~ 400 ppm, Fe, Hf, Si, Ca, Cr, etc.)
percentage of impurities 0.25% at most

Characteristics:

- Density – 6.48 g/cm³
- $H_\mu = 1148 \pm 34$ MPa
- Longitudinal sound velocity * - $c_l = 4684 \pm 6$ m/s
- Transverse sound velocity * - $c_s = 2331 \pm 3$ m/s
- Volume sound velocity - $c_0 = 3.83$ km/s

* sound velocity is given by the ultrasound method



Structure of alloy E100 (α -Zr – matrix (HCP crystalline lattice; grains size 3 μm ;

Lattice spacing in α -phase: $a = (0.3231 \pm 0.0001)$ nm, $c = (0.5147 \pm 0.0003)$ nm,
 $c/a = 1.593$; slitting of K_α into $K_{\alpha 1}$ and $K_{\alpha 2} \Rightarrow$ highly perfect structure;
above 610 °C ($\alpha \rightarrow \alpha + \beta$), above 890 °C ($\alpha + \beta \rightarrow \beta$).

Zirconium alloy E110



Composition:

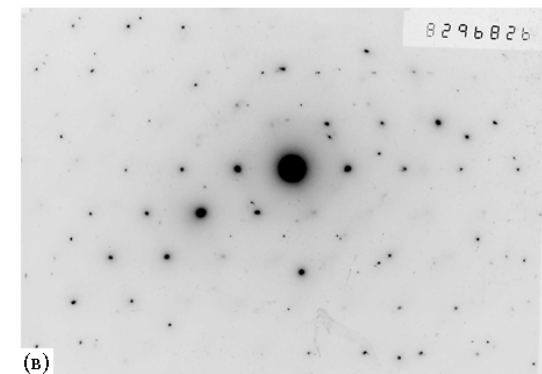
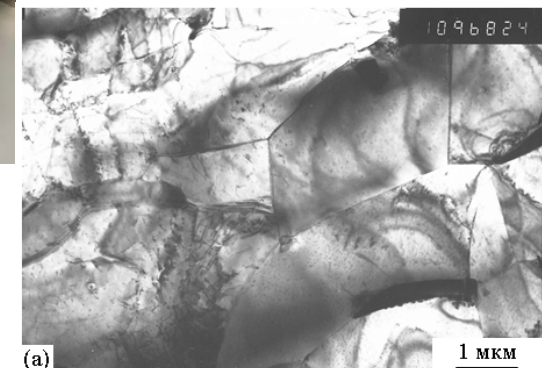
- Basic metal – Zirconium ($_{40}\text{Zr}$)
- Doped by Niobium ($_{41}\text{Nb}$) - 1%
- Impurities (O - 1300 ppm, Fe - 2400 ppm, Hf, Si, Ca, Cr, etc.) percentage of impurities 0.25% at most



Characteristics:

- Density – 6.5 g/cm³
- $H_\mu = 1649 \pm 55$ MPa ($\text{Zr} - H\mu = 1097 \pm 40$ MPa)
- Longitudinal sound velocity * - $c_l = 4703 \pm 15$ m/s
- Transverse sound velocity * - $c_s = 2262 \pm 5$ m/s
- Volume sound velocity - $c_0 = 3.91$ km/s

* sound velocity is given by the ultrasound method



Structure of alloy E110 (α -Zr – peaks of α -phase, faint peaks of β -phase zirconium+niobium \Rightarrow matrix of HCP lattice; enriched in niobium: α – phase $\sim 0.5\%$; β – phase - 17-18%;

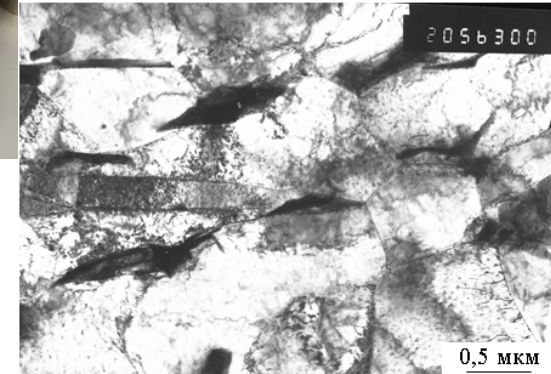
Grain size ~ 2 μm ; practically no dislocations)
above 610 °C ($\alpha \rightarrow \alpha + \beta$), above 890 °C ($\alpha + \beta \rightarrow \beta$).

Zirconium alloy E635



Composition:

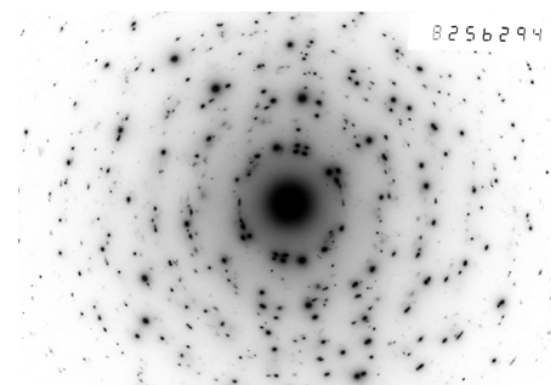
- Basic metal – Zirconium(₄₀Zr)
- Doped by Nb - 1%, Sn – (1.1-1.42) %,
 Fe – (0.3-0.47) %, O – (0.05-0.12) %
- Impurities – percentage of impurities 0.25% at most



Characteristics:

- Density – 6.5 g/cm³
- $H_{\mu} = 1755 \pm 49$ MPa
- Longitudinal sound velocity * - $c_l = 4711 \pm 12$ m/s
- Transverse sound velocity * - $c_s = 2274 \pm 2$ m/s
- Volume sound velocity - $c_0 = 3.91$ km/s

* sound velocity is given by the ultrasound method



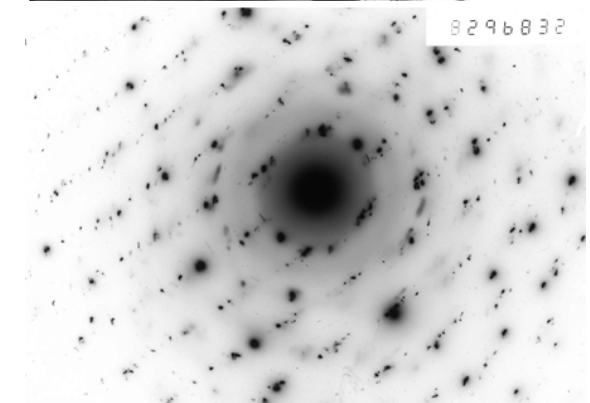
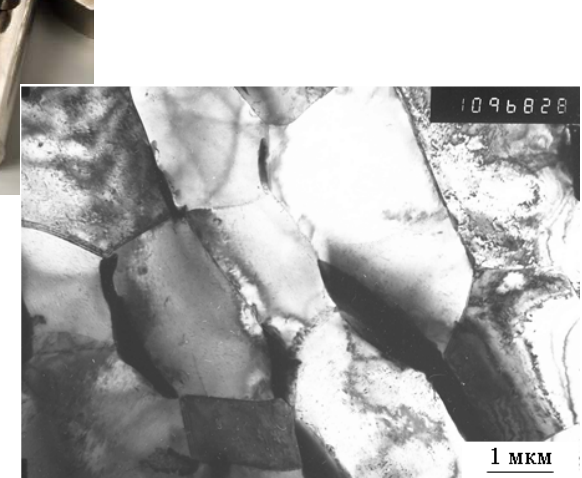
X-ray diffraction analysis showed the test material to be a hetero-phase material.

Structure: α -Zr – matrix (HCP crystalline lattice; small share of β – phase (BCC-lattice) in layers along boundaries of α – phase; small amount of micro-twins and individual dislocations;

+ [1] intermetallics $Zr(Nb,Fe)_2$ (HCP) and $(Zr,Nb)_2Fe$ (FCC)

1. Nikulina A.V., Markelov V.A., Peregud M.M. et al. 11th International Symposium. ASTM STP 1295. 1996. P. 785-804.

Zirconium alloy E125



Composition:

- Basic metal – Zirconium ($_{40}\text{Zr}$)
- Doped by Niobium ($_{41}\text{Nb}$) – 2,5 %
- Impurities (O - 2400 ppm, Fe, Hf, Si, Ca, Cr, etc.)
percentage of impurities 0.27% at most

Characteristics:

- Density – 6.54 g/cm³
- $H_\mu = 1873 \pm 53$ МПа ($H\bar{\mu} = 1565 \pm 140$ MPa)
- Longitudinal sound velocity * - $c_l = 4636 \pm 3$ m/s
- Transverse sound velocity * - $c_s = 2221 \pm 1$ m/s
- Volume sound velocity - $c_o = 3.86$ km/s

* sound velocity is given by the ultrasound method

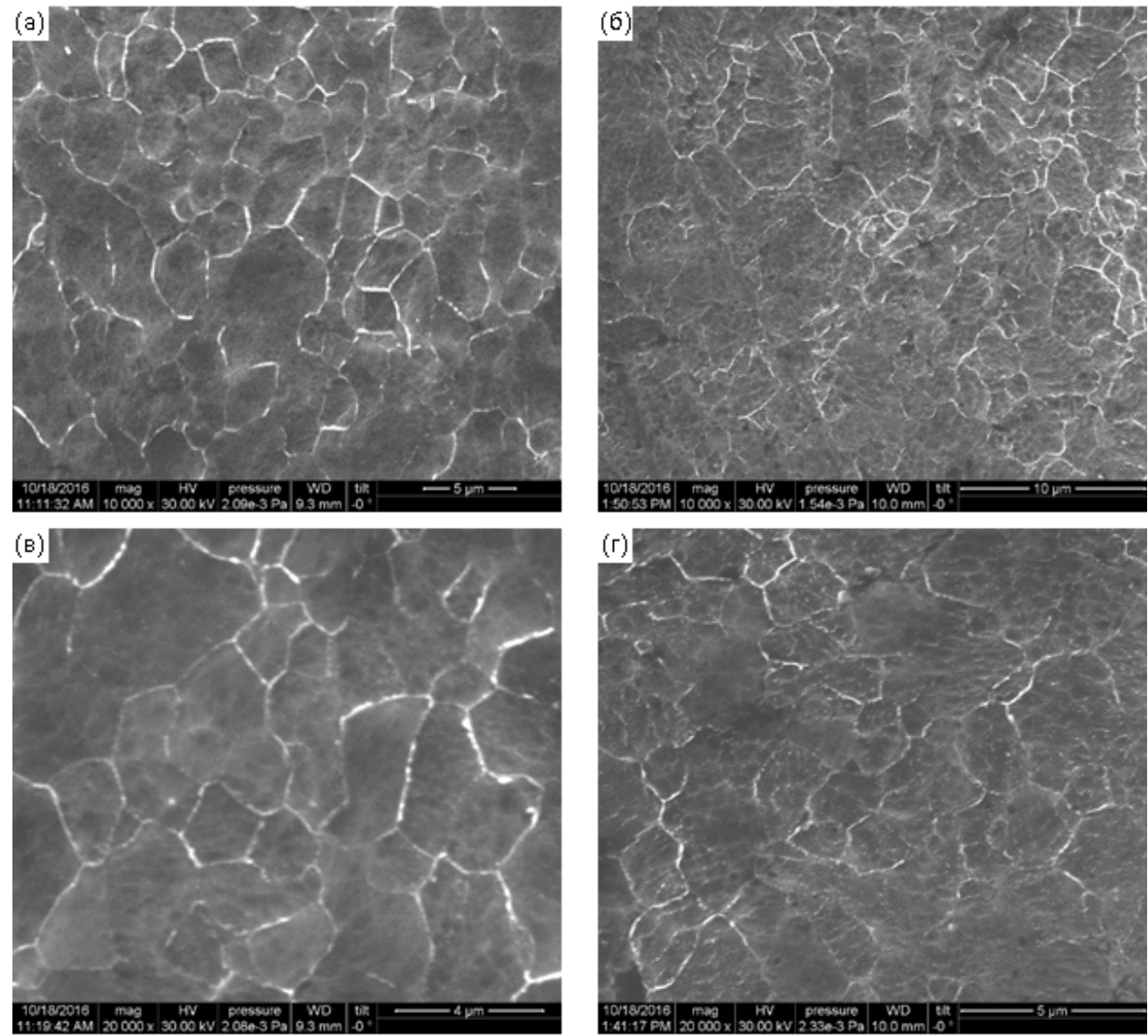
Structure of alloy E125 (α -Zr – matrix, ГПУ решетка; grains size is 1..3 μm ;
small share of β – phase, enriched up to 18% niobium:
diffraction peaks of α -phase, faint peaks of β -phase zirconium+ niobium
above 610 °C ($\alpha \rightarrow \alpha + \beta$), above 890 °C ($\alpha + \beta \rightarrow \beta$).

Initial structure of alloy E100 (bar Ø40)



(a), (c) – longitudinal section;

(b), (d) – transverse section



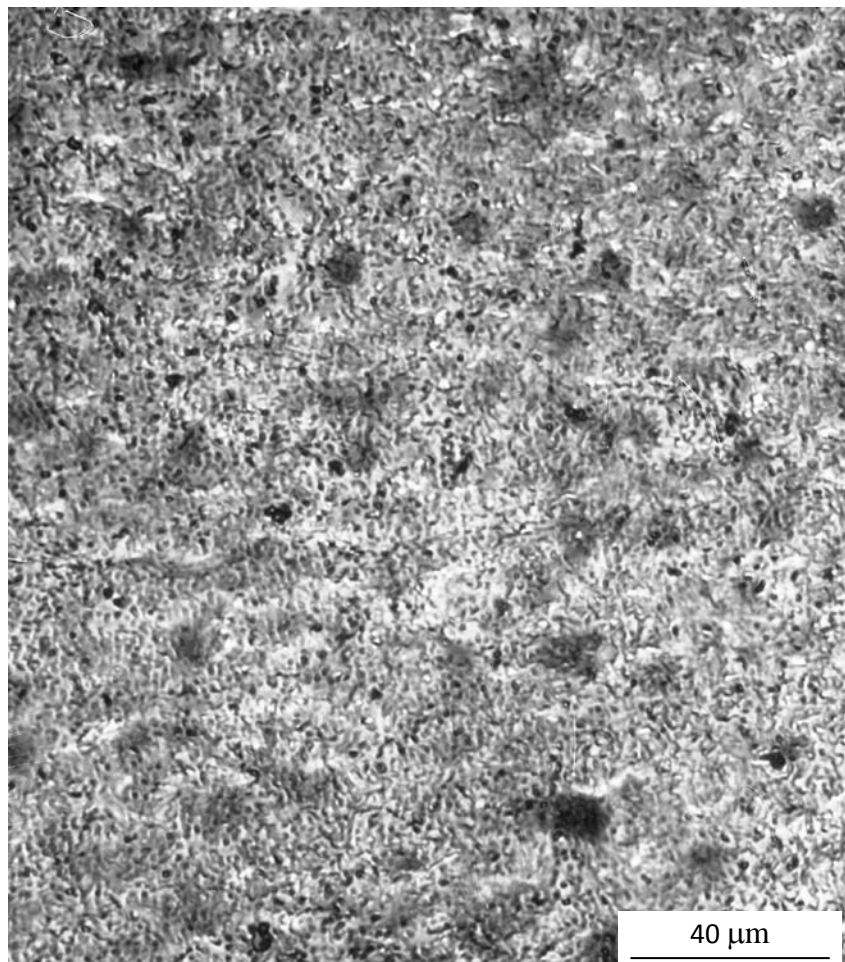
Initial structure of alloys Zr-1%Nb



E110

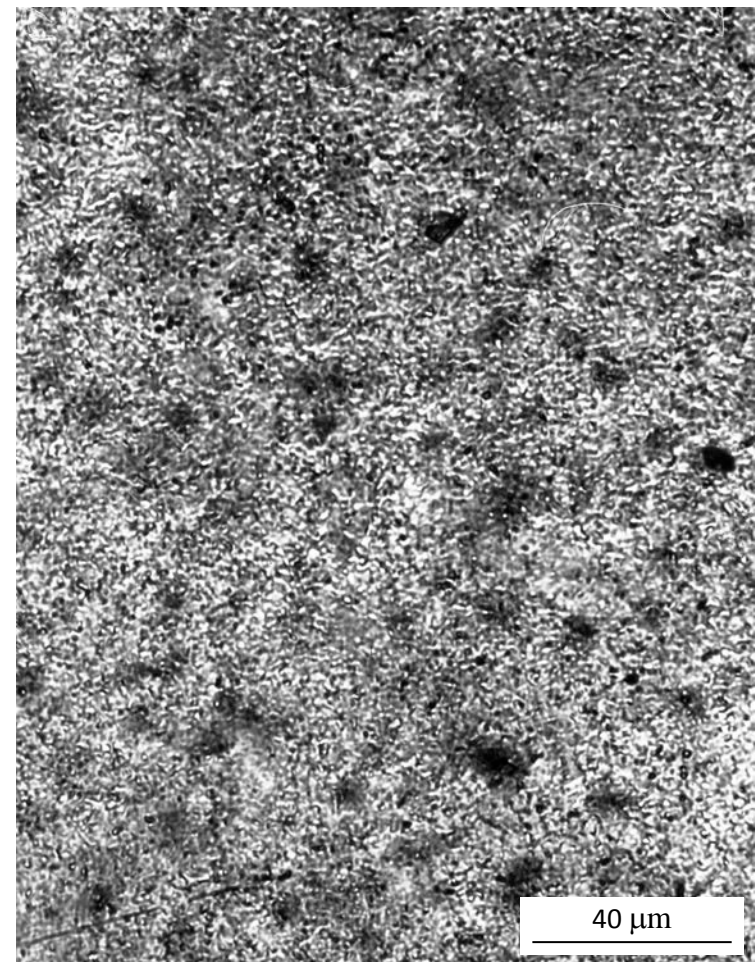
Transverse section

E635



$H_\mu = 1649 \pm 55 \text{ MPa}$

Bar Ø35



$H_\mu = 1755 \pm 49 \text{ MPa}$

Initial structure of alloys Zr-1%Nb



E110

Longitudinal section

E635



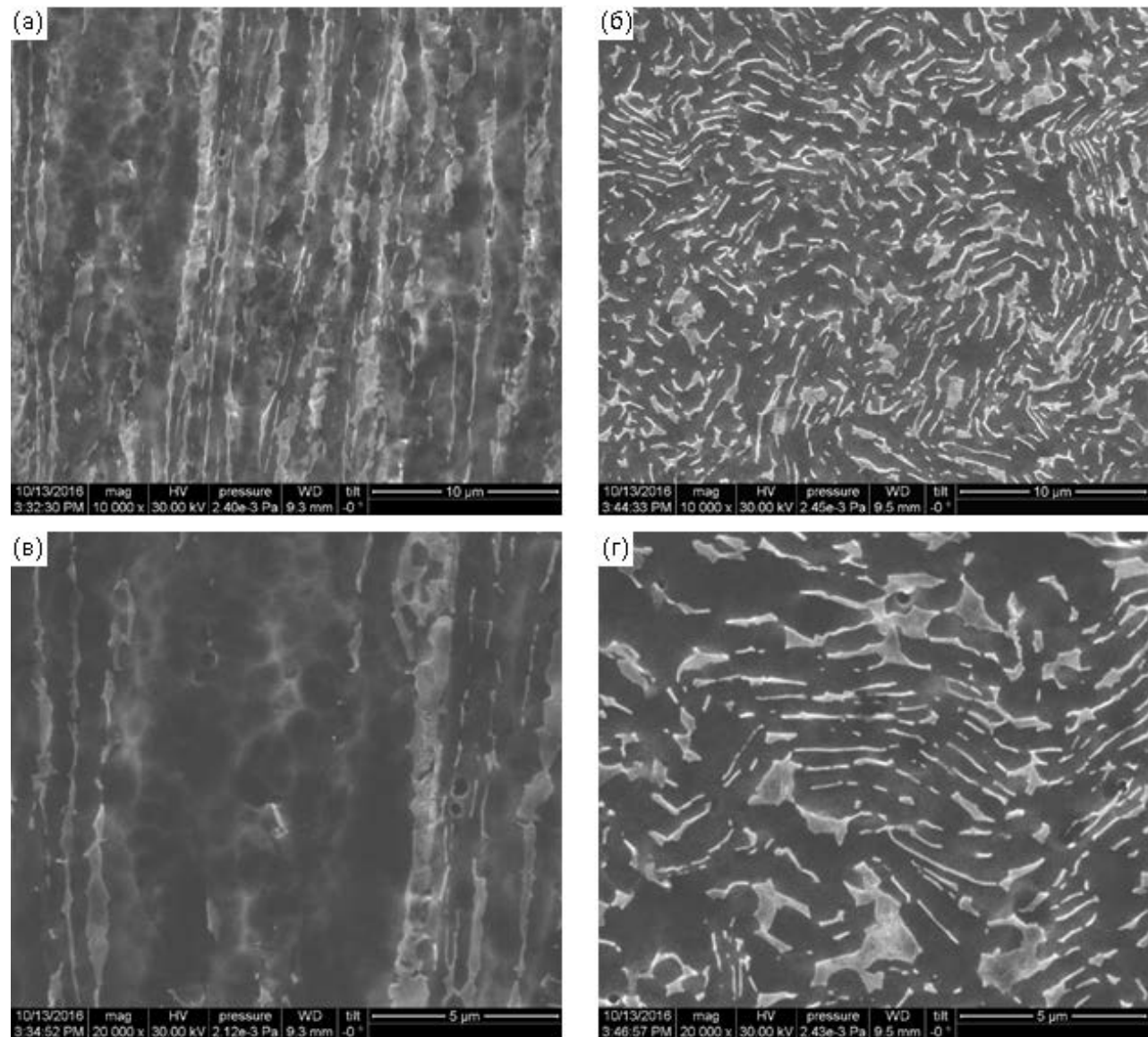
XRD patterns demonstrate diffraction peaks of α -phase, as well as faint peaks of zirconium β -phase enriched in niobium

Initial structure of alloy E125 (bar Ø34)

(a), (d) – longitudinal section;

(b), (c) – transverse section

XRD patterns demonstrate diffraction peaks of α -phase, as well as faint peaks of zirconium β -phase enriched in 18 % niobium; β -phase is found along α -phase grain boundaries and in triple joints

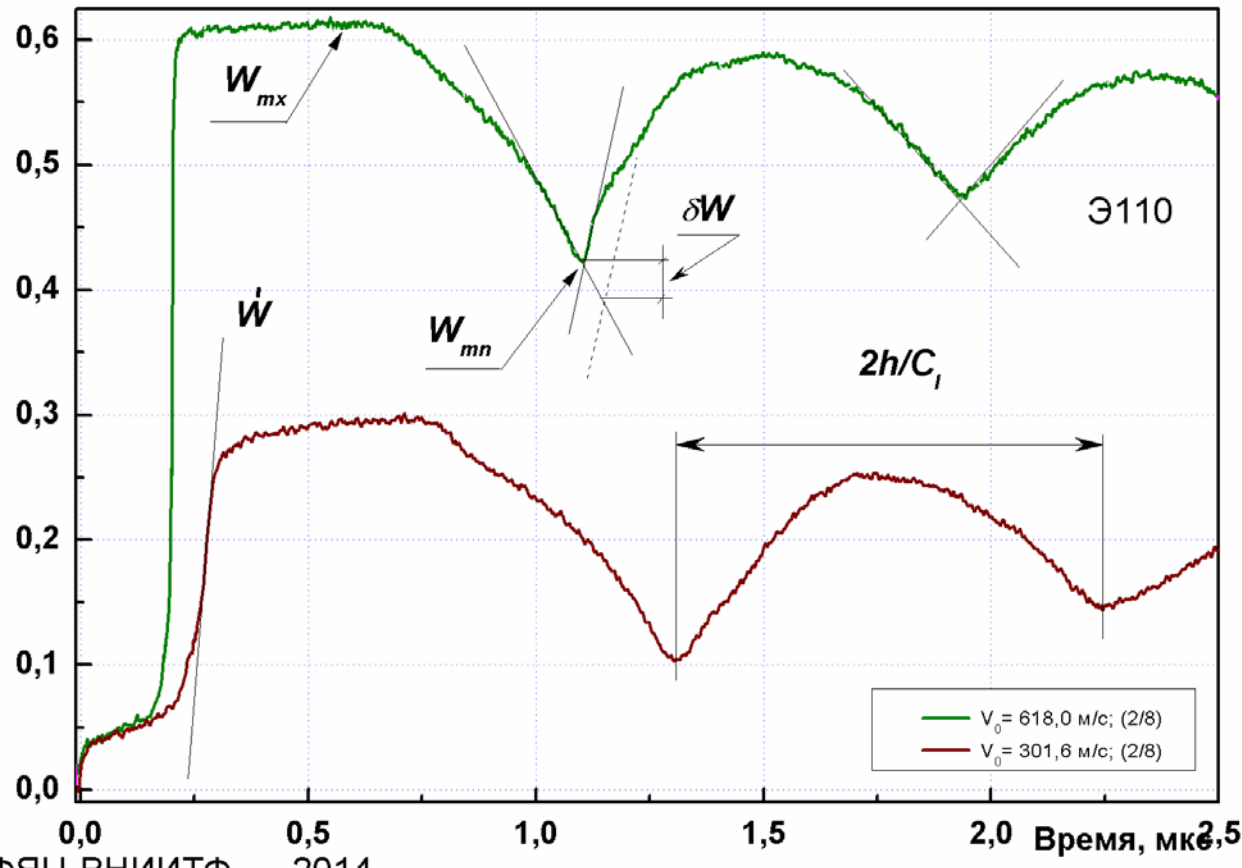


Shock wave profiles



Канель Г.И.

Искажение волновых профилей при отколе в упругопластическом теле. ПМТФ, том 42, №2, с. 194-198, 2001.



РФНЦ-ВНИИТФ

Забабахин Е.И.

Некоторые вопросы газодинамики взрыва. Снежинск, 1997.

Канель Г.И., Фортов В.Е., Разоренов С.В., Уткин А.В.

Ударно-волновые явления в конденсированных средах. Москва, М: Янус-К, 1996.

$$\sigma^* = \rho_0 c_b (\Delta u_{fs} + \delta)/2.$$

$$c_F = c_b c_l \sqrt{\frac{\dot{\sigma}_x^+ - \dot{\sigma}_x^-}{\dot{\sigma}_x^+ c_l^2 - \dot{\sigma}_x^- c_b^2}},$$

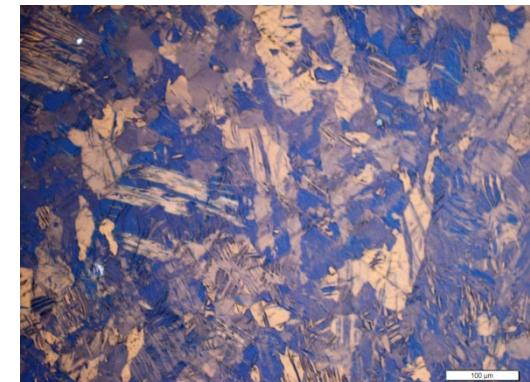
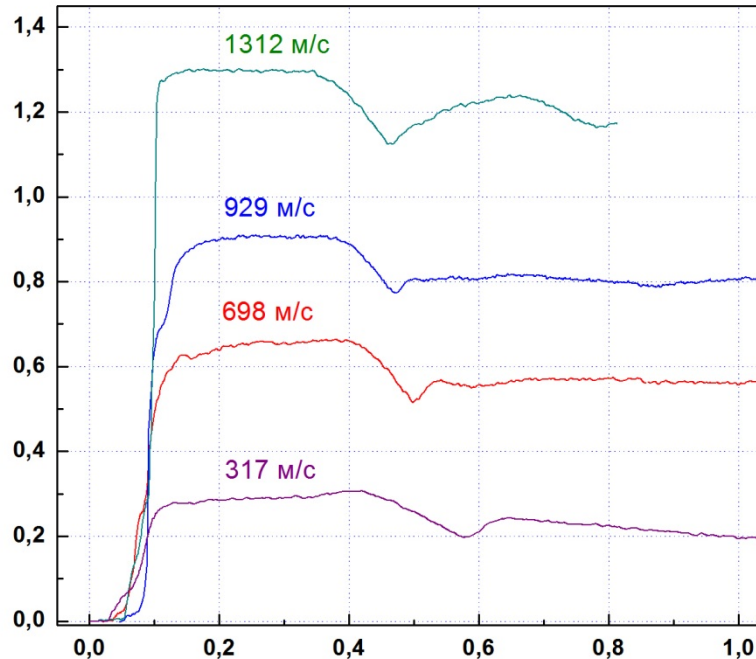
$$\delta = (h/c_b - h/c_F)|\dot{u}_1|$$

$$\delta = \left(\frac{h}{c_b} - \frac{h}{c_l} \right) \frac{|\dot{u}_1 \dot{u}_2|}{|\dot{u}_1| + \dot{u}_2}.$$

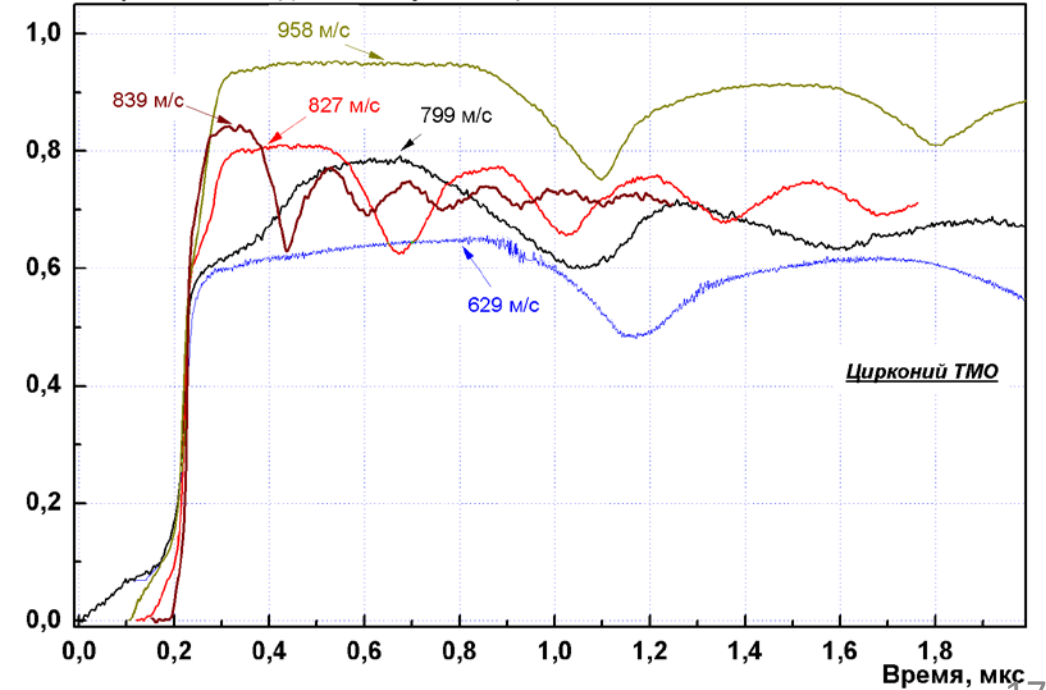
Experimental Results. Zirconium (iodine)



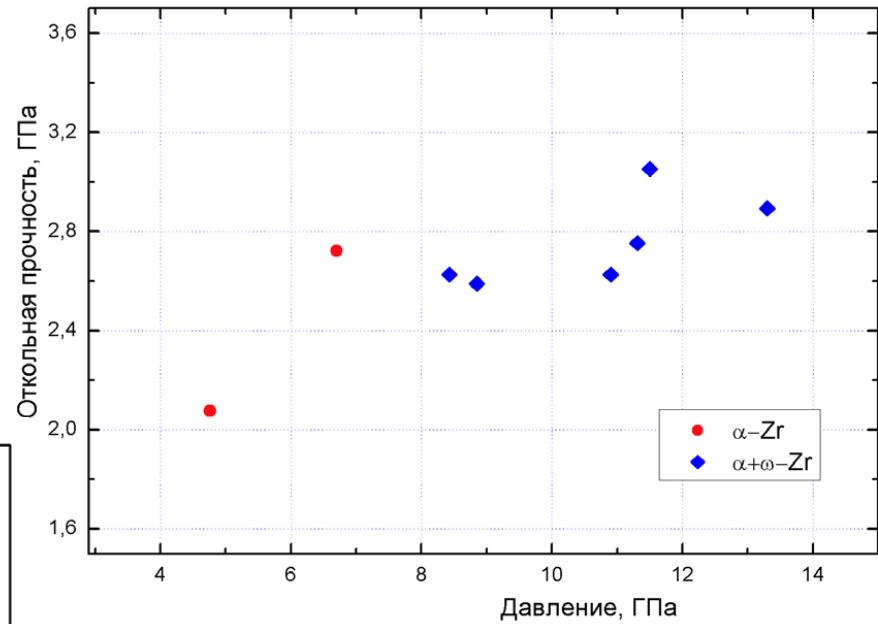
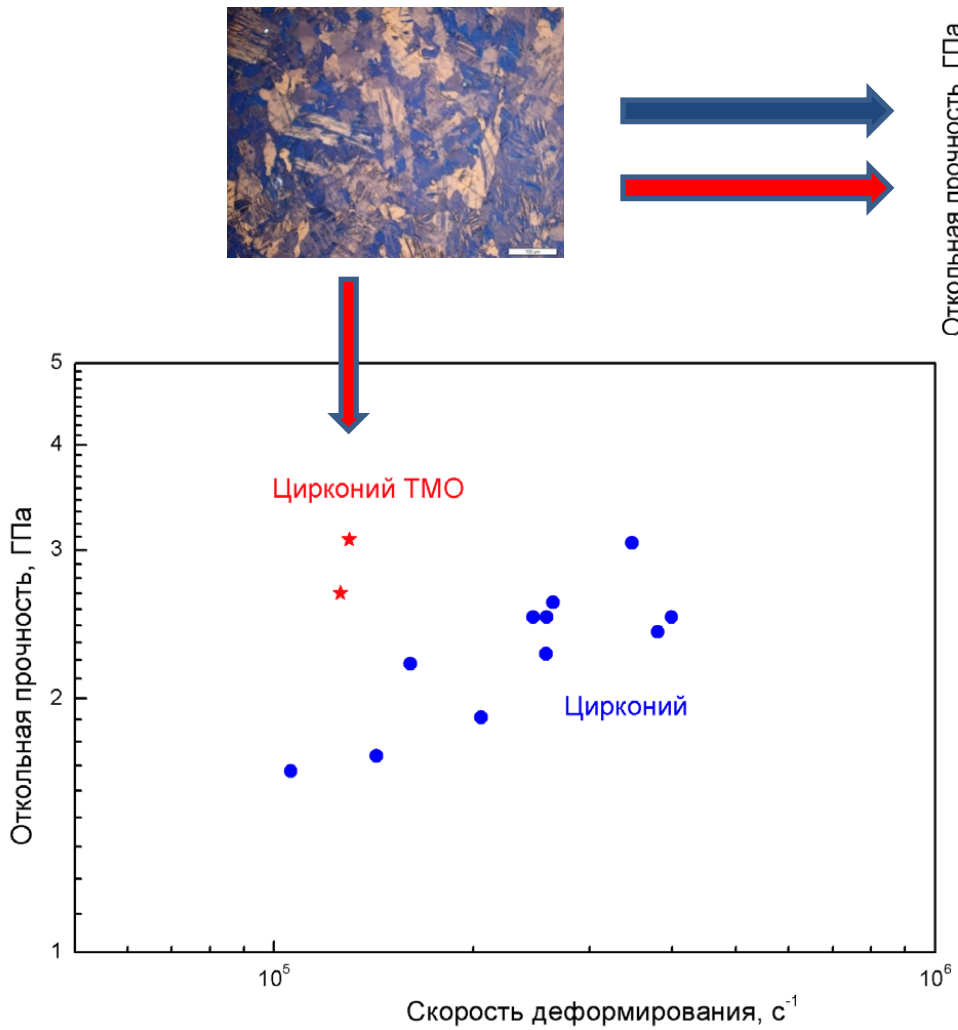
Скорость свободной поверхности, км/с



Скорость свободной поверхности, км/с



Experimental results Zirconium (iodine)

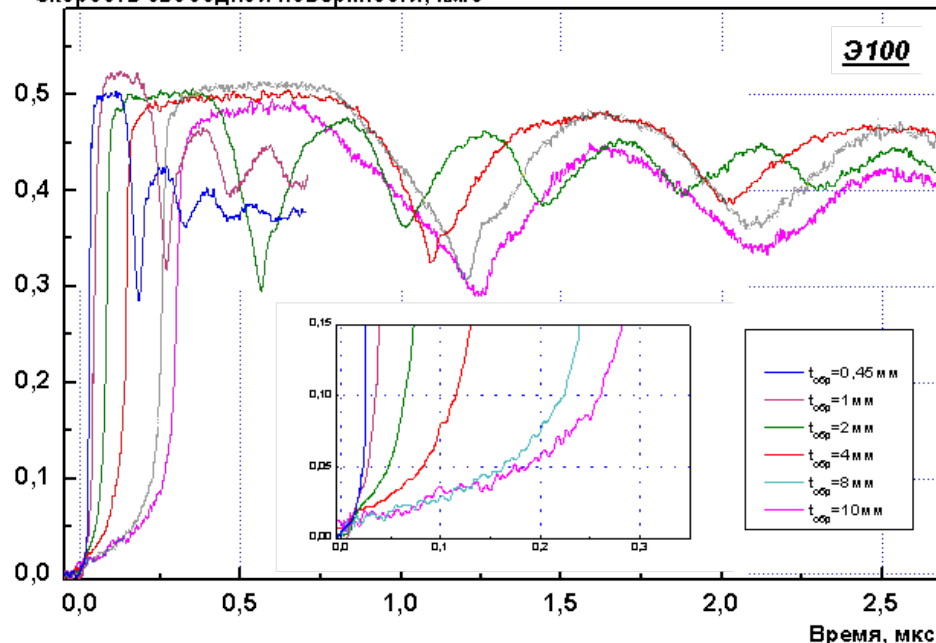


Shock loading duration:
from ~ 0.05 to $1 \mu\text{s}$

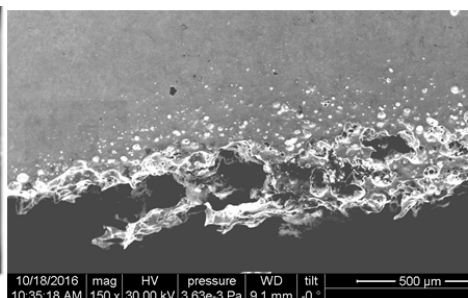
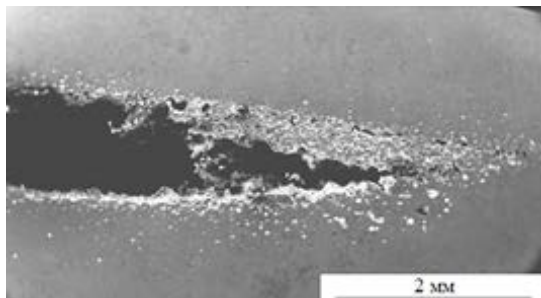
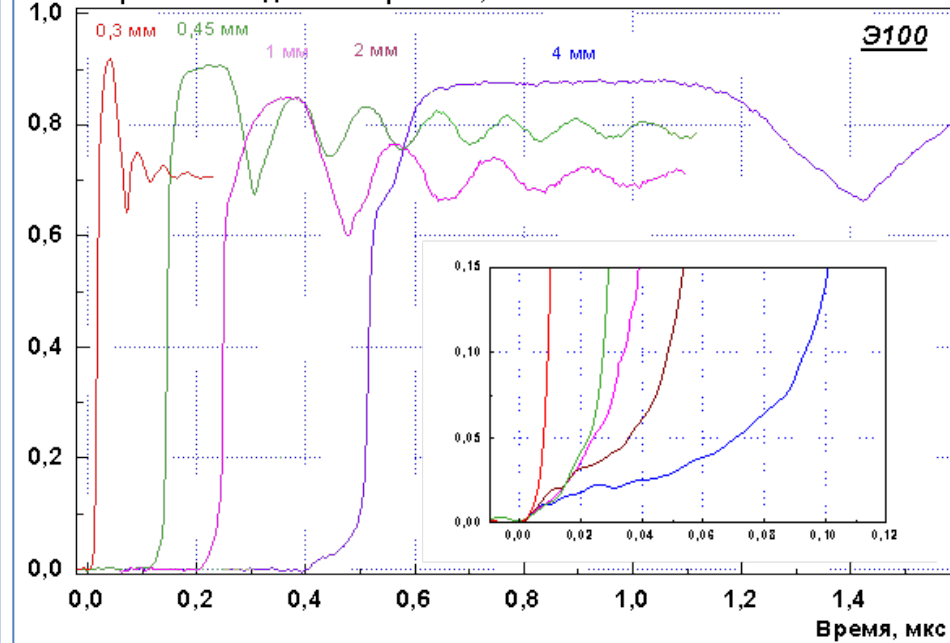
Measurement Results Zirconium Alloy E100



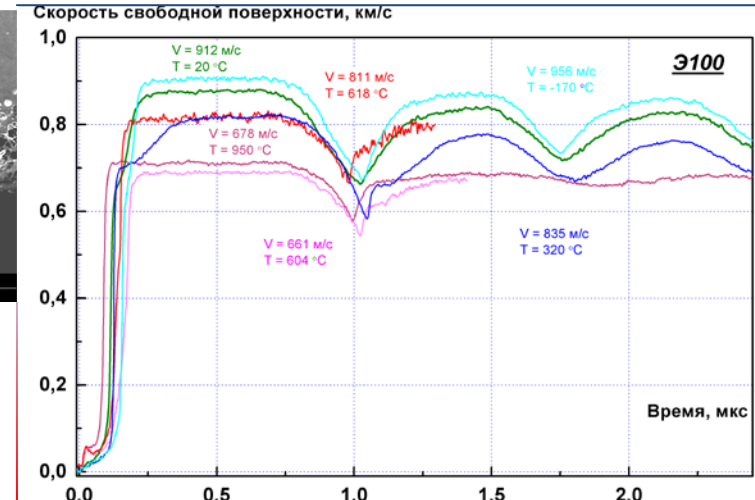
Скорость свободной поверхности, км/с



Скорость свободной поверхности, км/с



$$D = 3.83 + 0.91u$$

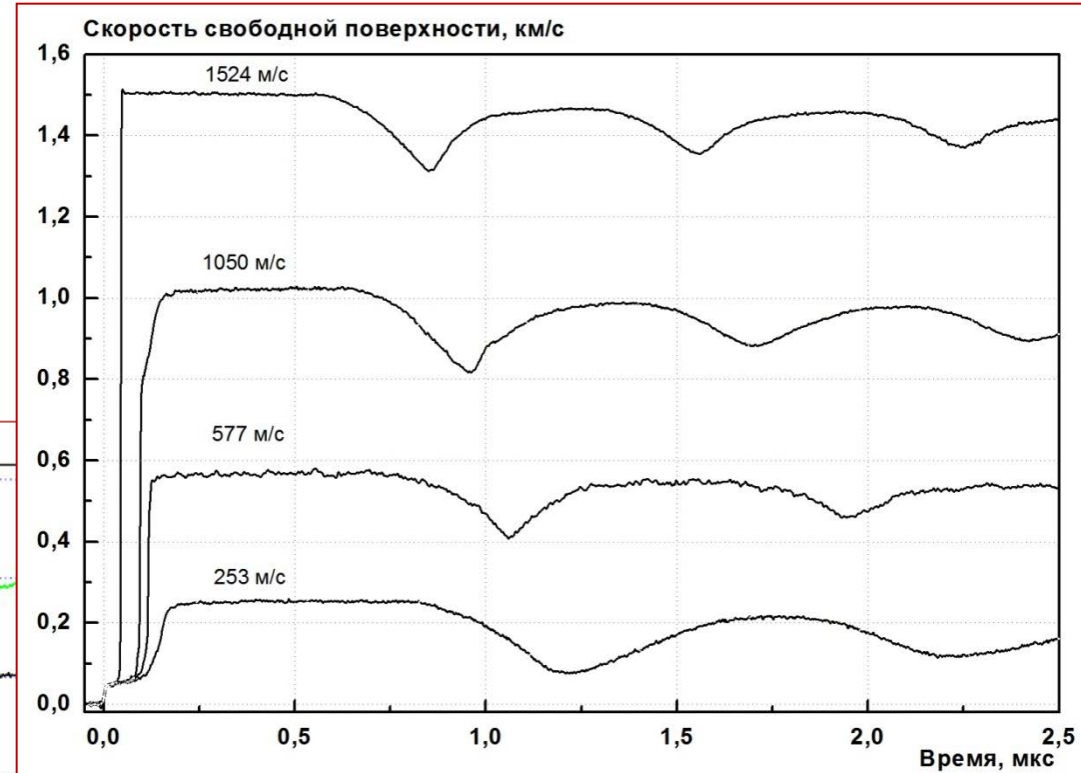
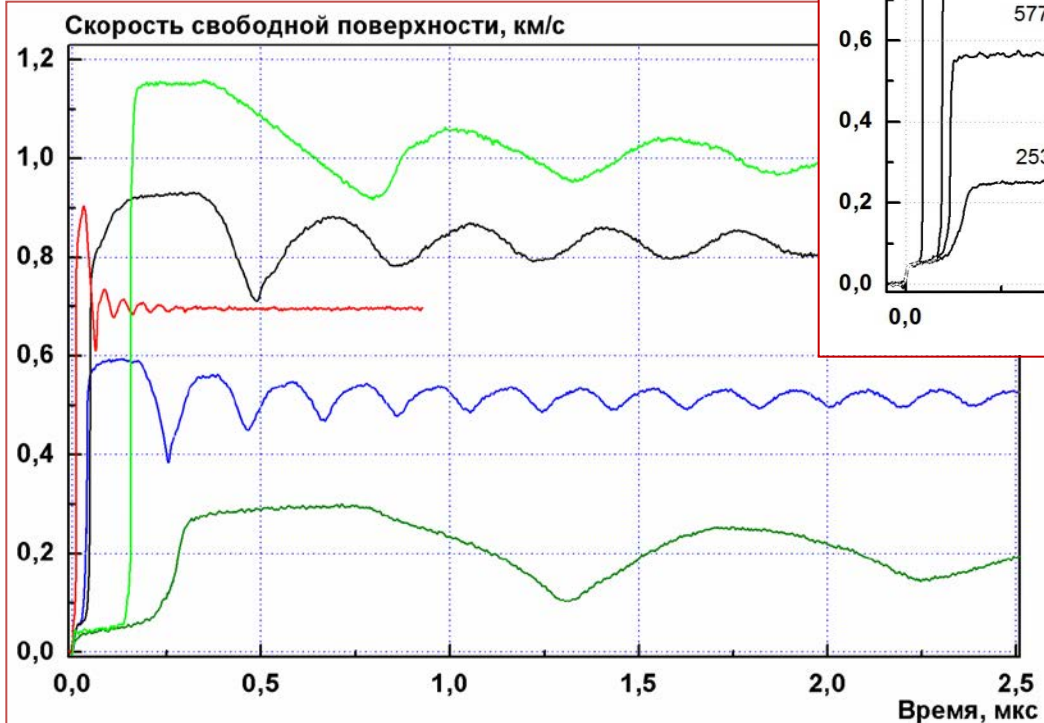


Measurement Results Zr-1%Nb Zirconium alloy E110



$$D = 3.91 + 0.91u$$

Loading amplitude:
from 3.4 to 23 GPa

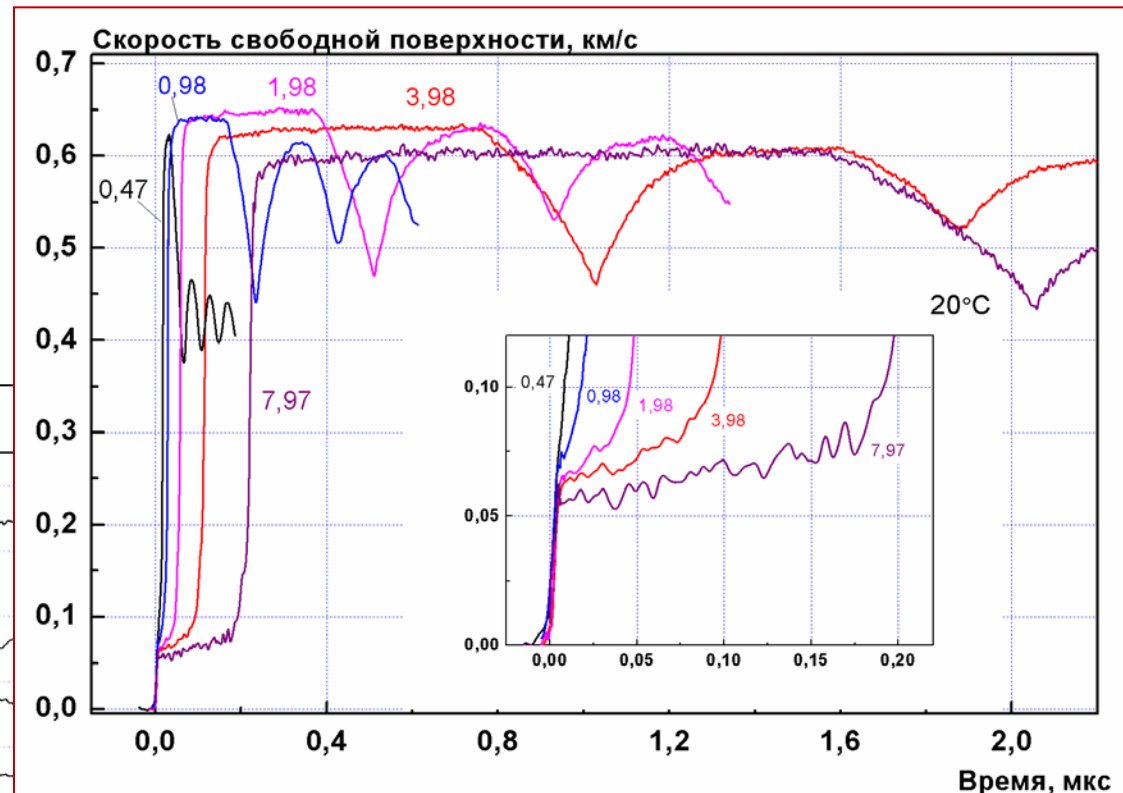
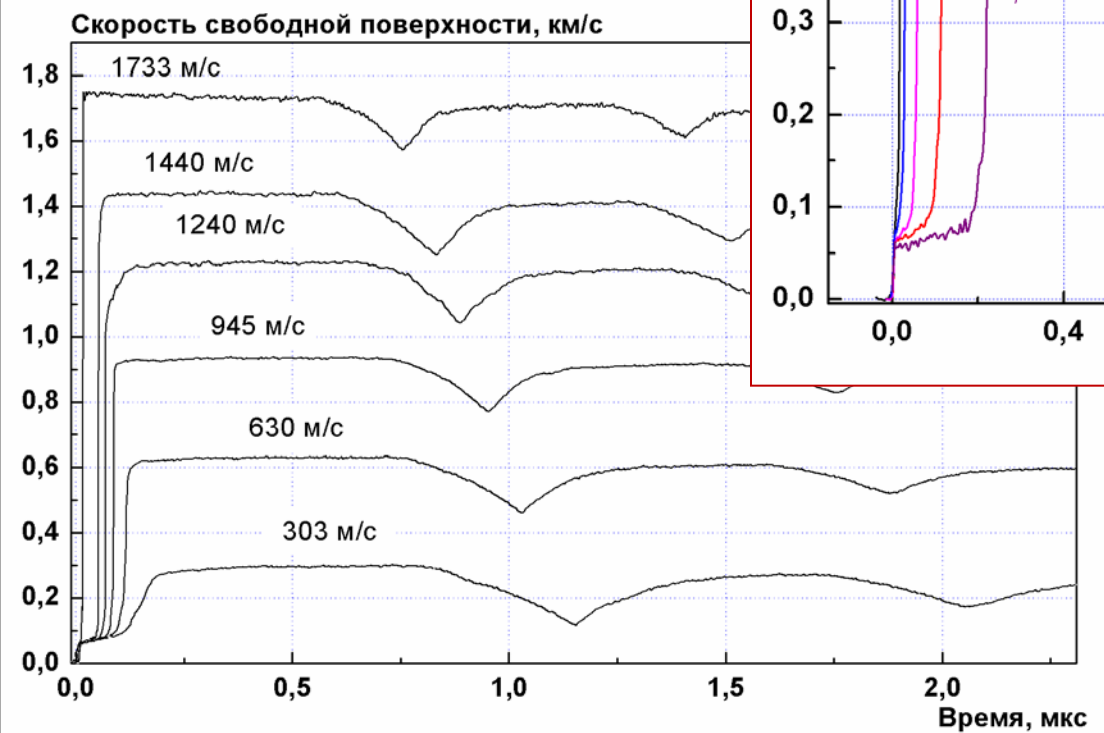


Shock loading duration:
from ~ 0.05 to 1 μ s

Measurement Results Zr-1%Nb Zirconium alloy E635



Shock loading duration:
from ~0.05 to ~2 μ s



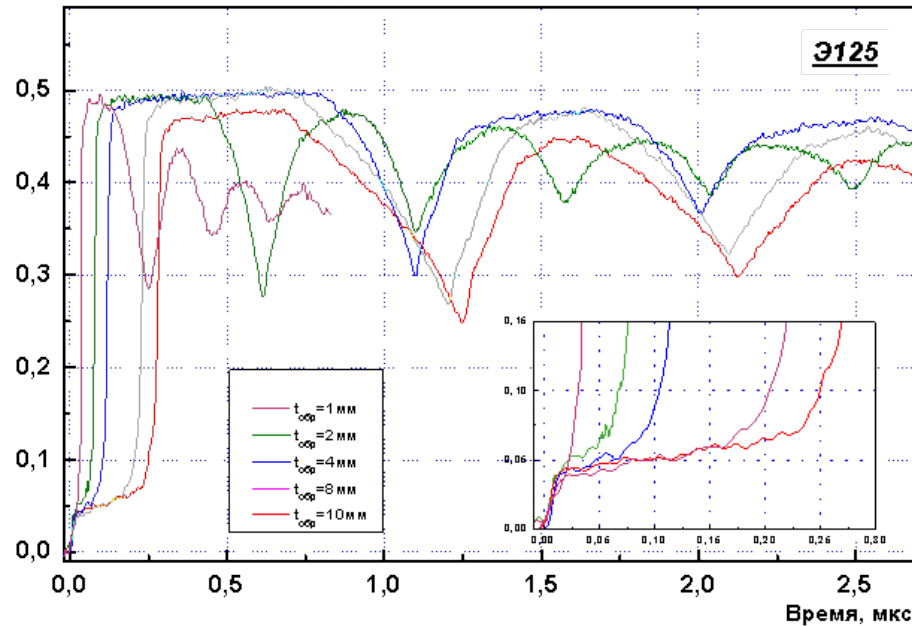
$$D = 3.91 + 0.91u$$

Loading amplitude:
from 4 to 26 GPa

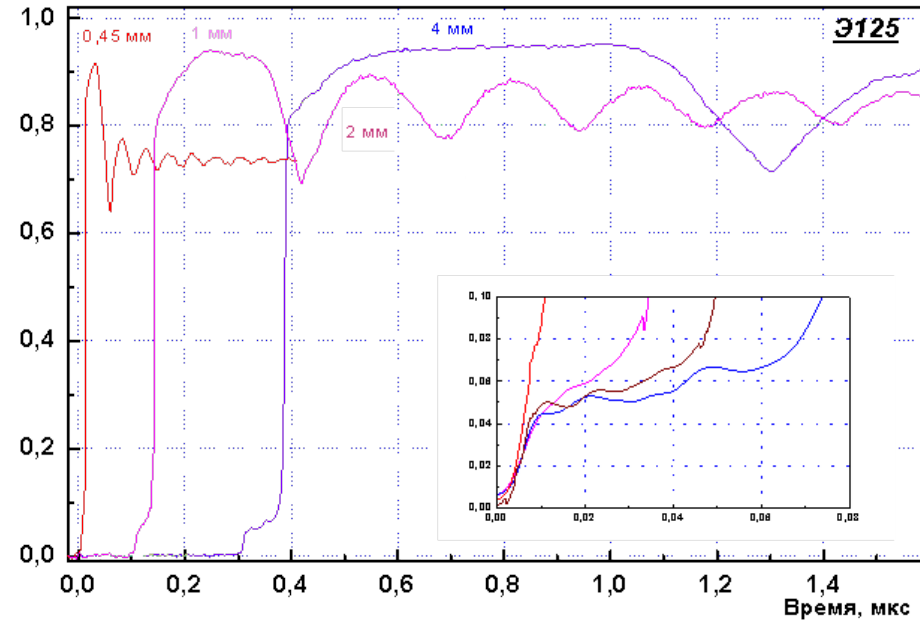
Measurement Results Zr-2,5%Nb Zirconium alloy E125



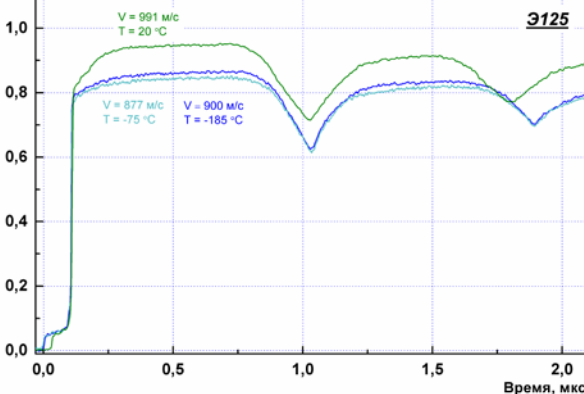
Скорость свободной поверхности, км/с



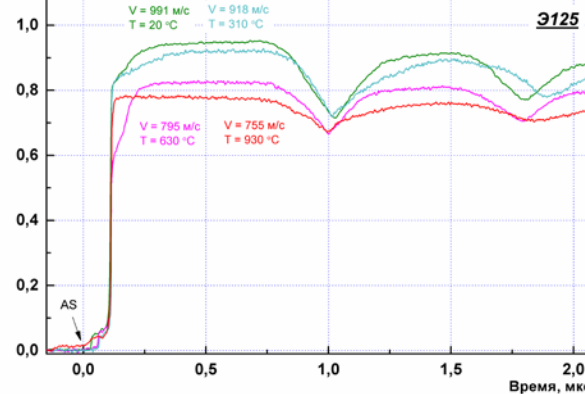
Скорость свободной поверхности, км/с



Скорость свободной поверхности, км/с



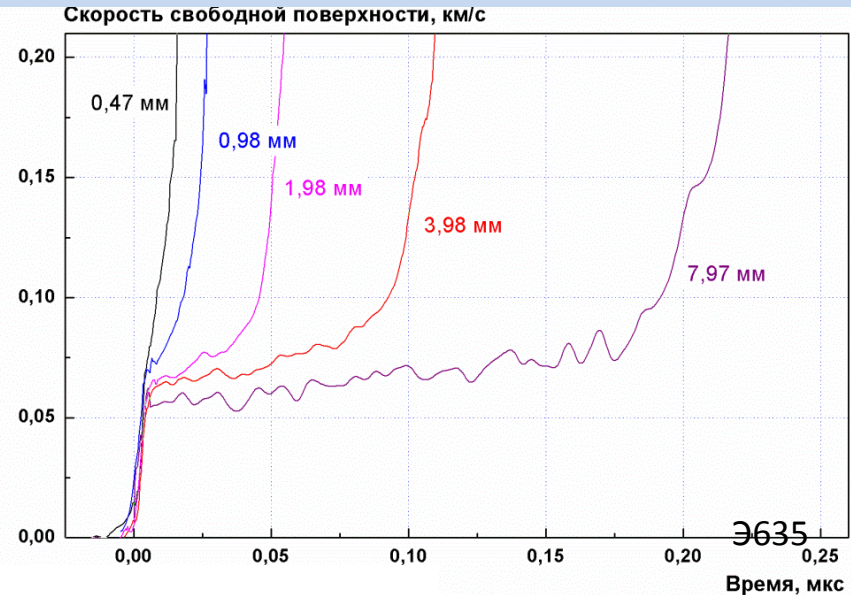
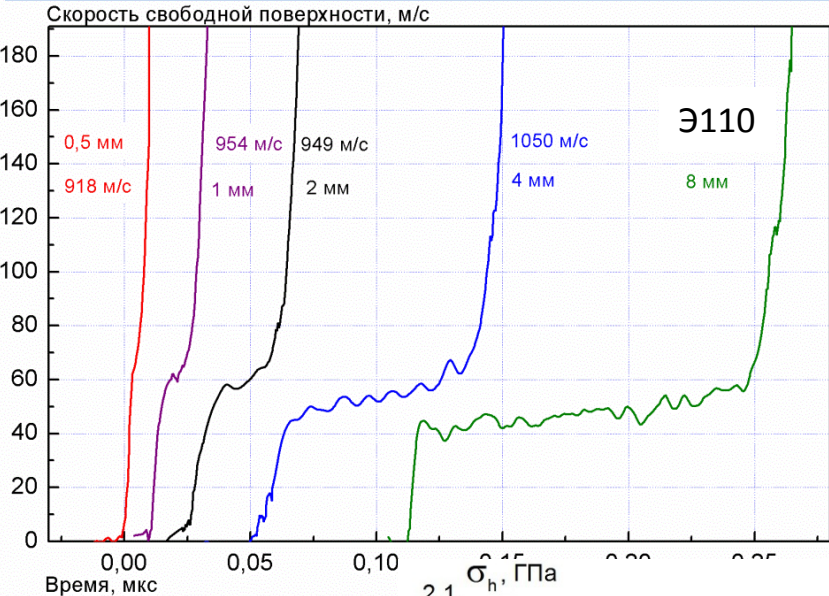
Скорость свободной поверхности, км/с



$$D = 3.86 + 0.91u$$

Shock loading duration:
from ~ 0.05 to $1 \mu\text{s}$

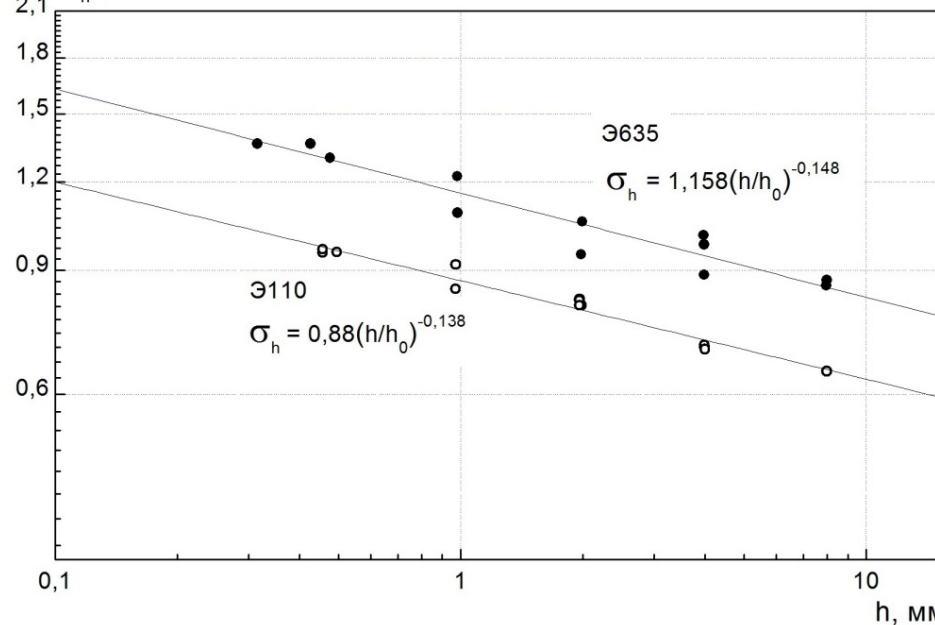
Relaxation of Elastic Precursor



$$\sigma_h = \rho_0 c_l W_h / 2$$

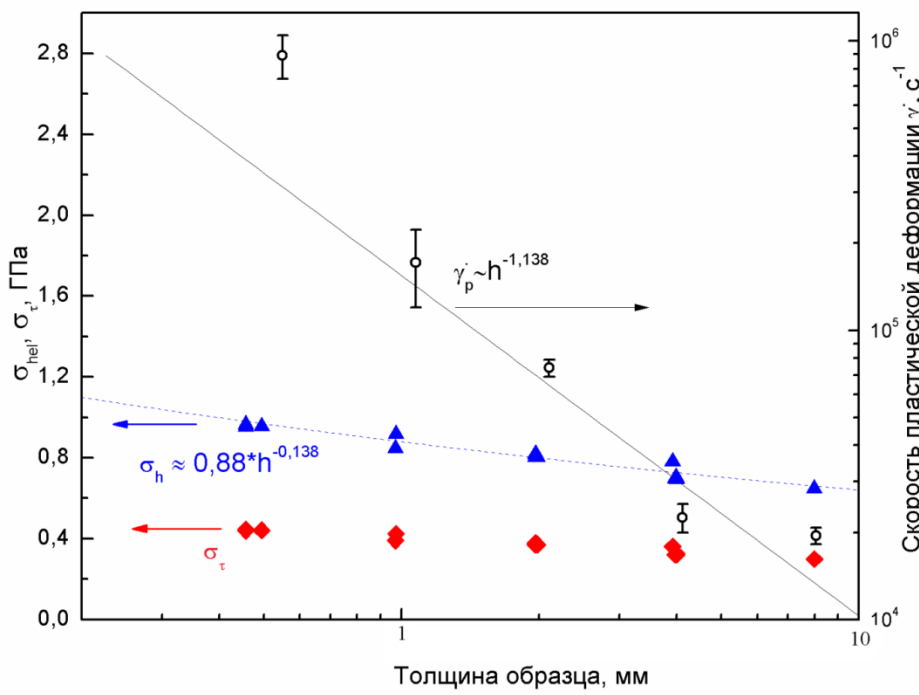
$$\sigma_h = S(h/h_0)^{-\alpha}$$

$$h_0 = 1 \text{ mm}$$



	E635	E110
S	1.158	0.88
α	0.148	0.138

E110: Elastic Precursor Relaxation and Plastic Strain Rate



$$\left. \frac{d\sigma_x}{dh} \right|_{\text{HEL}} = - \frac{S\alpha}{h_0} \left(\frac{h}{h_0} \right)^{-(\alpha+1)}$$

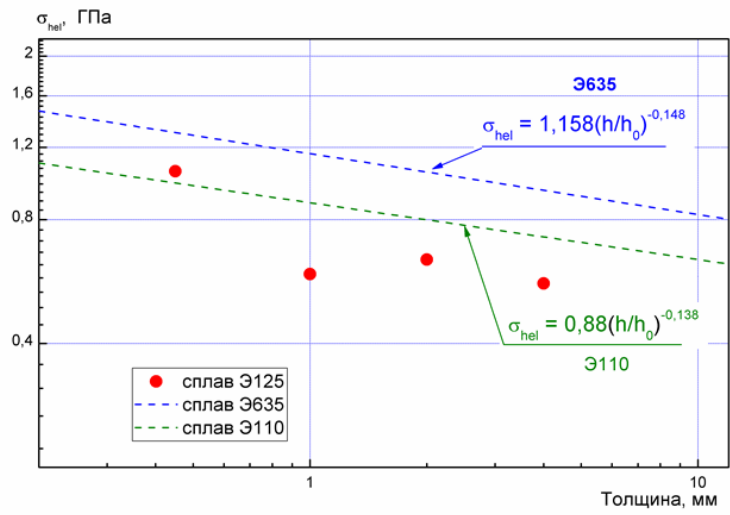
$$\dot{\gamma}_p = \frac{3}{4} \frac{S\alpha c_l (h/h_0)^{-(\alpha+1)}}{h_0 G}$$

$$\left. \frac{d\sigma_x}{dh} \right|_{\text{HEL}} = - \rho_0 \frac{\partial u}{\partial t} + \frac{1}{c_l} \frac{\partial \sigma_x}{\partial t}$$

$$\left. \frac{du}{dt} \right|_{\text{HEL}} = \rho_0 \frac{\partial V}{\partial t} + \frac{1}{c_l} \frac{\partial u}{\partial t}$$

$$\left. \frac{d\sigma_x}{dh} \right|_{\text{HEL}} = - \frac{4}{3} \frac{G \dot{\gamma}_p}{c_l}$$

$$\sigma_h = S(h/h_0)^{-\alpha}$$

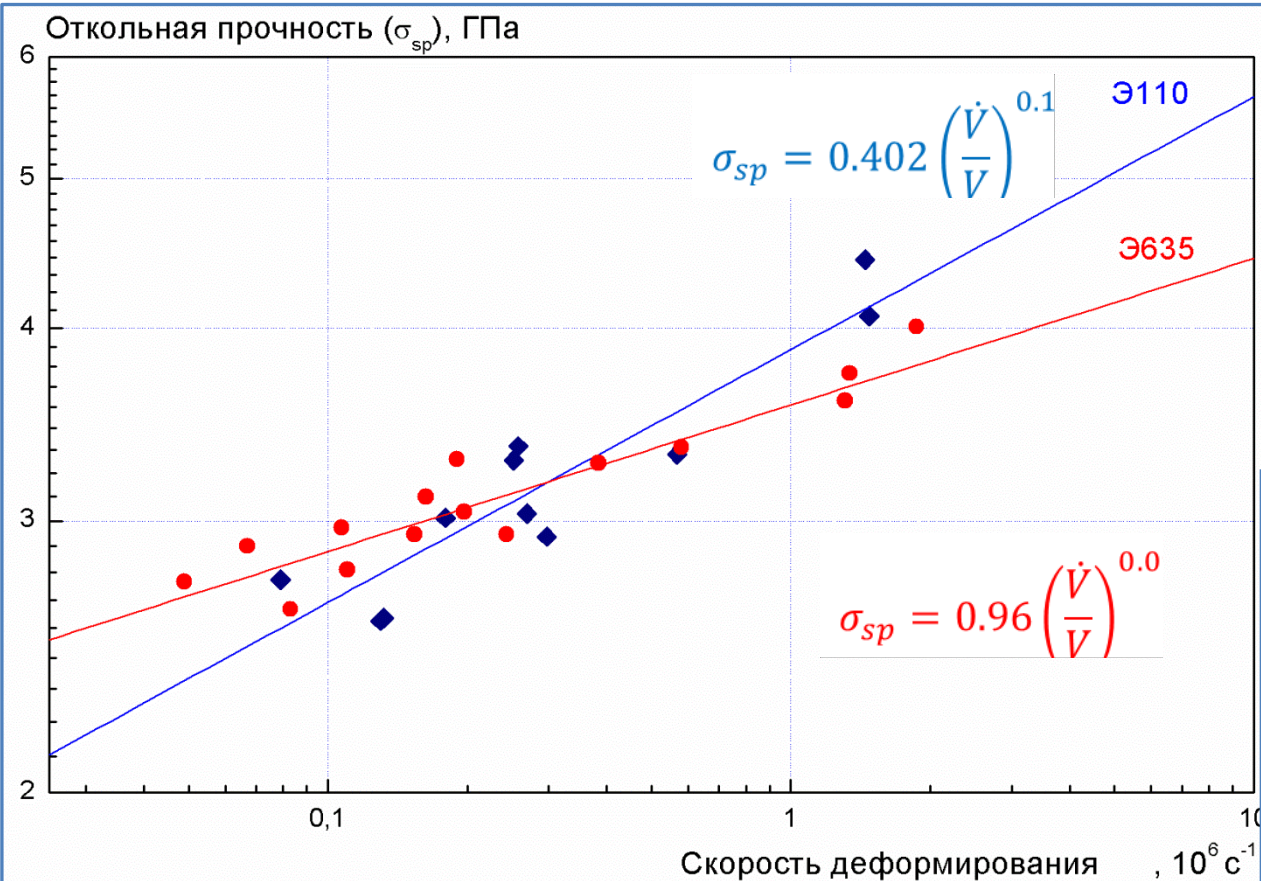


- G.E. Duvall. In: Stress Waves in Inelastic Solids, edited by H. Kolsky and W. Prager, 1964
- Ahrens T.J. and Duvall G.E. *J. Geophys. Res.*, **71**(18), 4349-4360 (1966).
- J. R. Asay, G. R. Fowles, and Y. Gupta, *J. Appl. Phys.* **43**, 744 (1972).
- Г.В. Гаркушин, Г.И. Канель, С.В. Разоренов. ФТТ, 2012. Т. 54, №5.

Spall strength



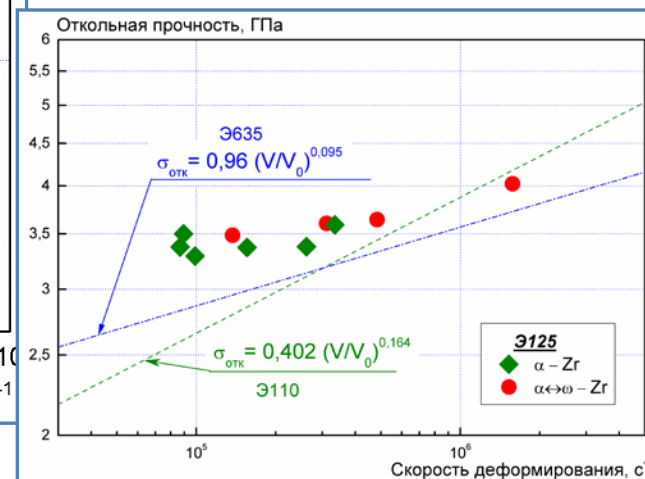
Alloys Zr – 1% Nb



Zirconium (E100)



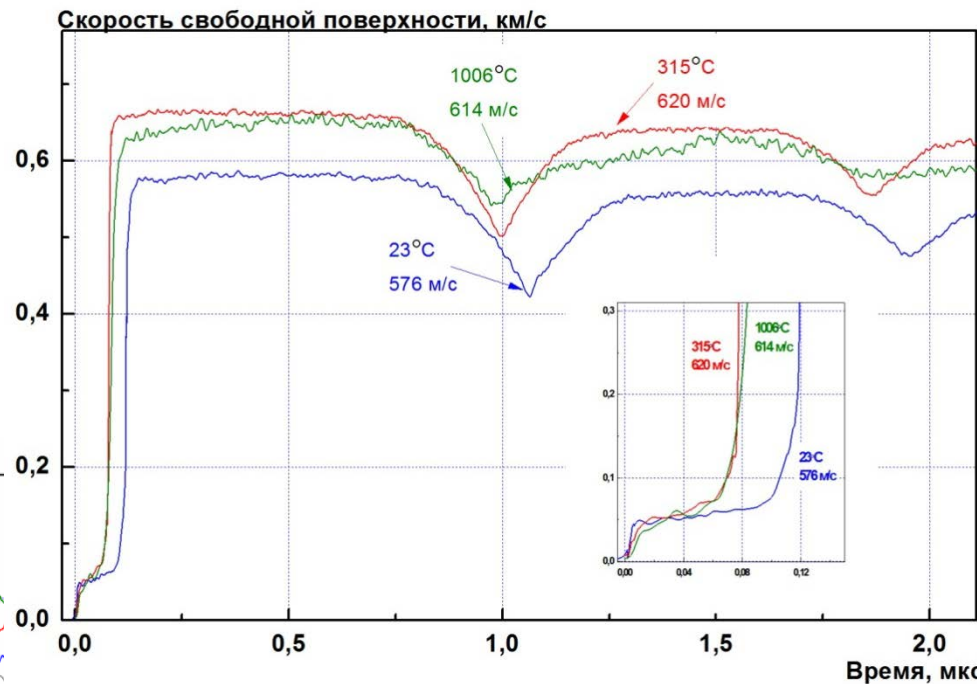
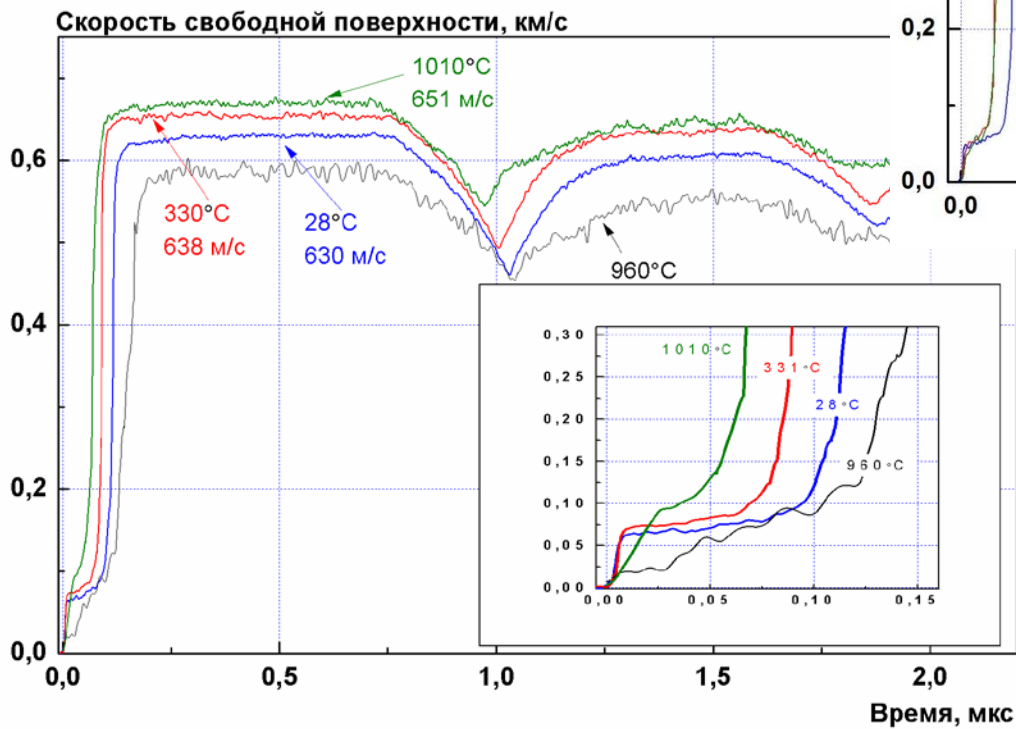
Alloy Zr – 2,5 % Nb



Elevated temperatures. Alloys E635 and ЕЭ110

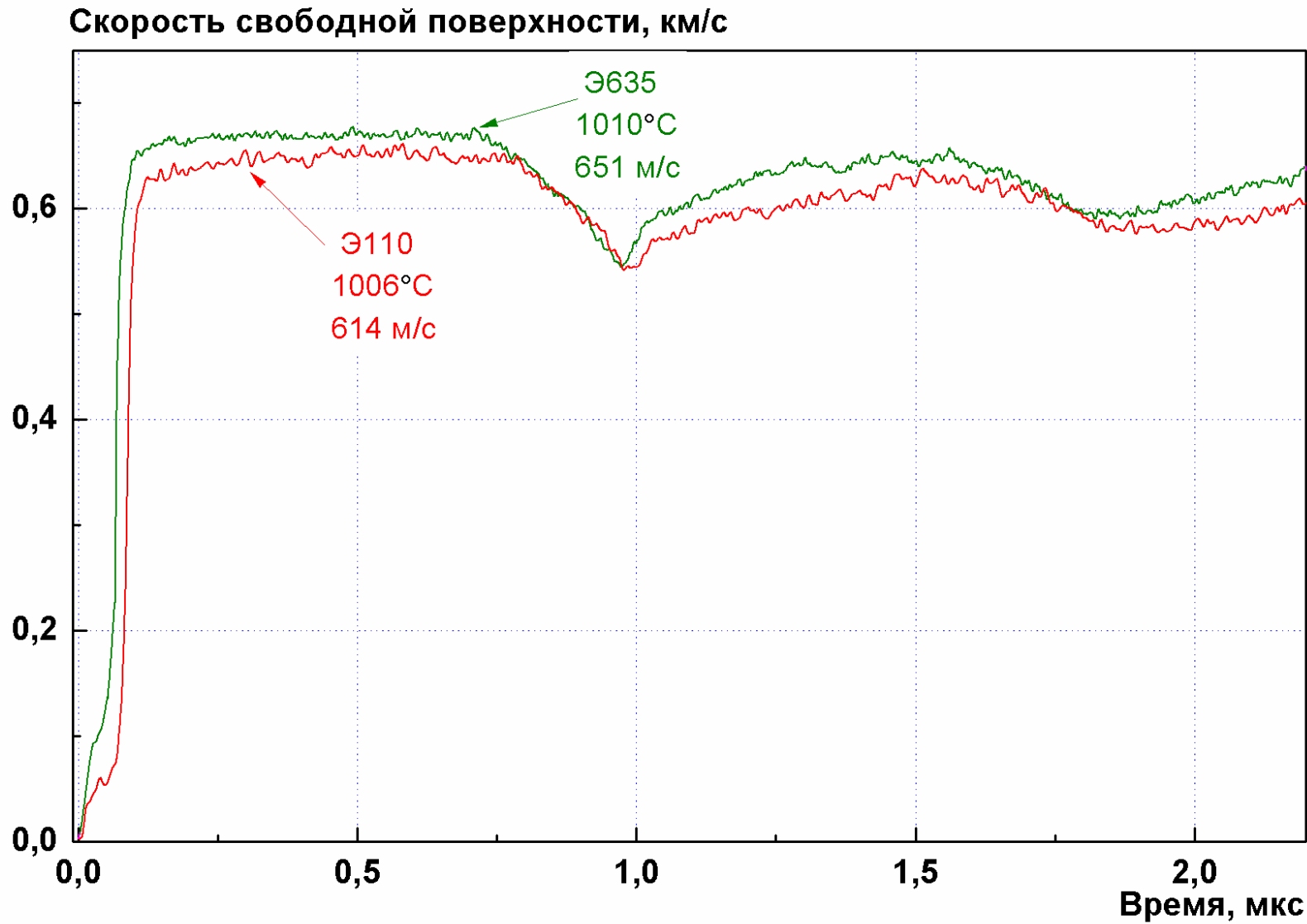


E635	28° C	330°C	960°C	1010°C
σ_h, MPa	980	1090	-	1420
σ, GPa	2.8	2.7	2.3	2.0



E110	23° C	315°C	1006°C
σ_h, MPa	640	710	703
σ, GPa	2.7	2.6	1.8

Alloys E635 and E110



Temperature dependence of spall strength



Zirconium (E100)

Alloy Zr – 2.5 % Nb (E125)

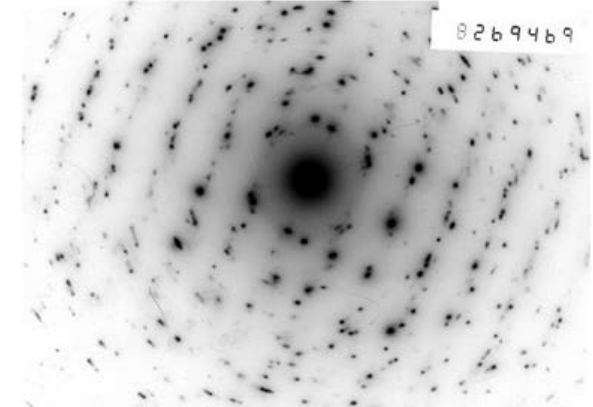
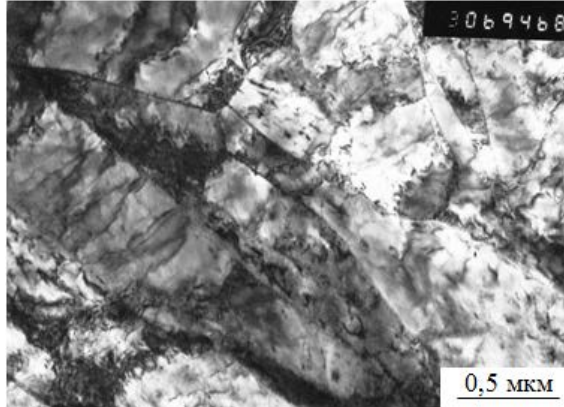
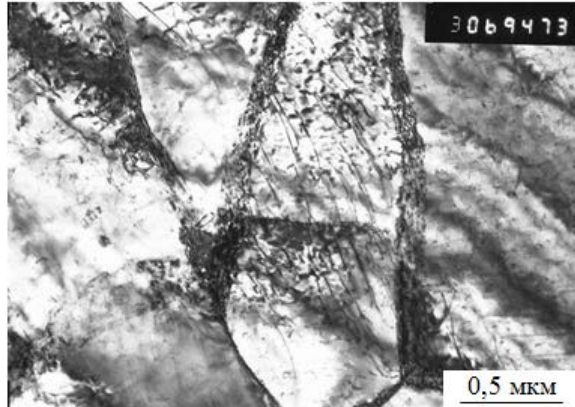


Zirconium E100 (recovered samples)

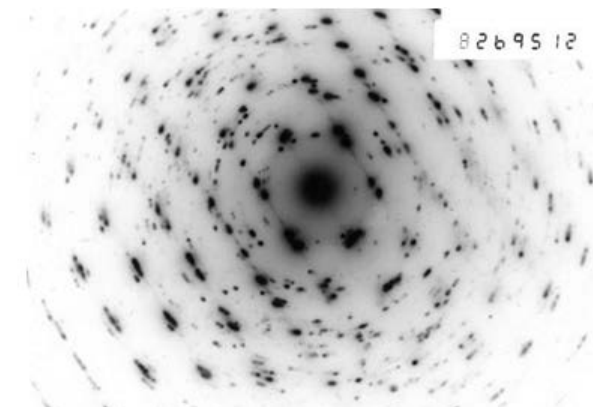
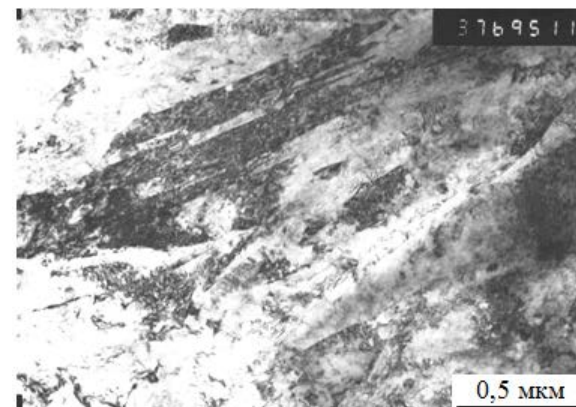
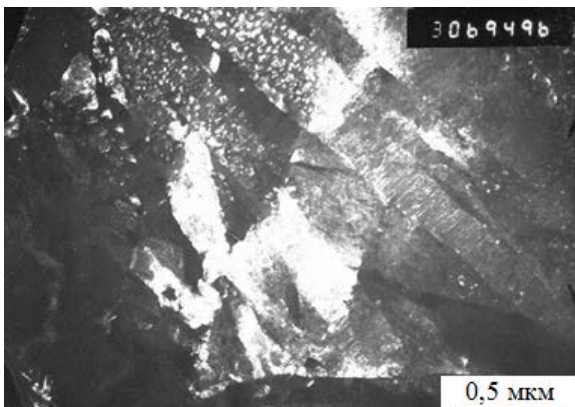


V = 0.5 km/s

Deformation structure has great many dislocations (scattered, dislocation boundaries)



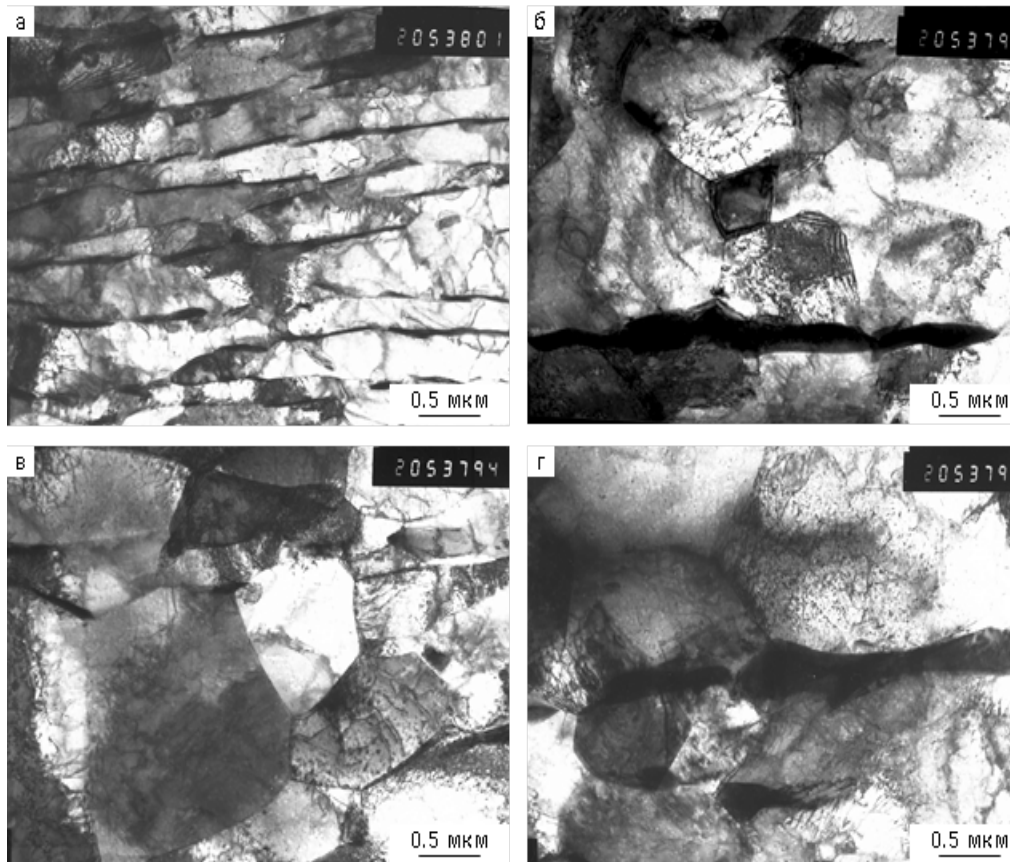
V = 0.9 km/s



$\alpha \leftrightarrow \omega$ phase transition, ω -phase is recovered in the metastable state;
available reflexes of ω -phase and diffuse scatter strands, specific striped contrast

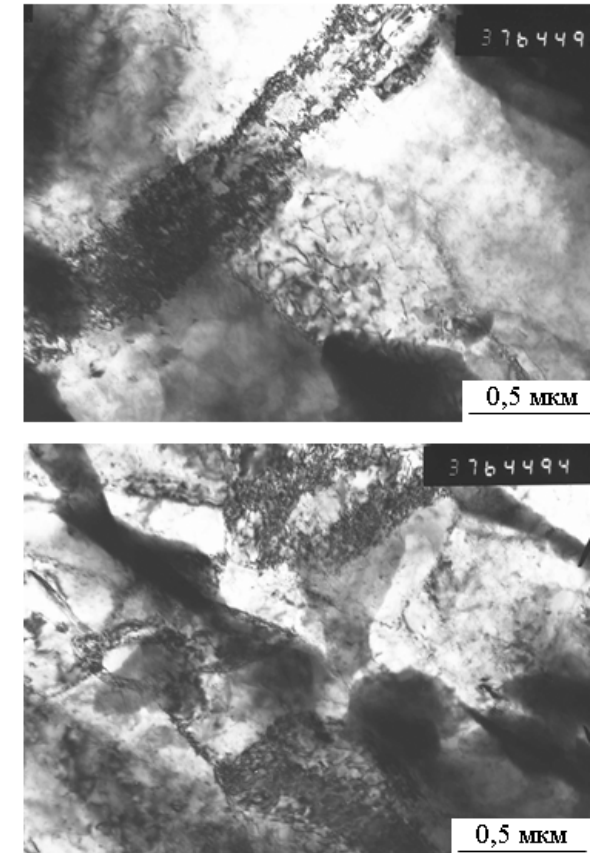
Microstructure of alloy E110 (samples recovered after loading)

No micro-twins, β - phase is available along α - phase grain boundaries, a parent grain undergoes fragmentation with the formation of uniaxial grains and plate-like grains, low density of dislocations



$V = 0.21 \text{ km/s}; T = 600^\circ\text{C}$

$V = 0.58 \text{ km/s}$



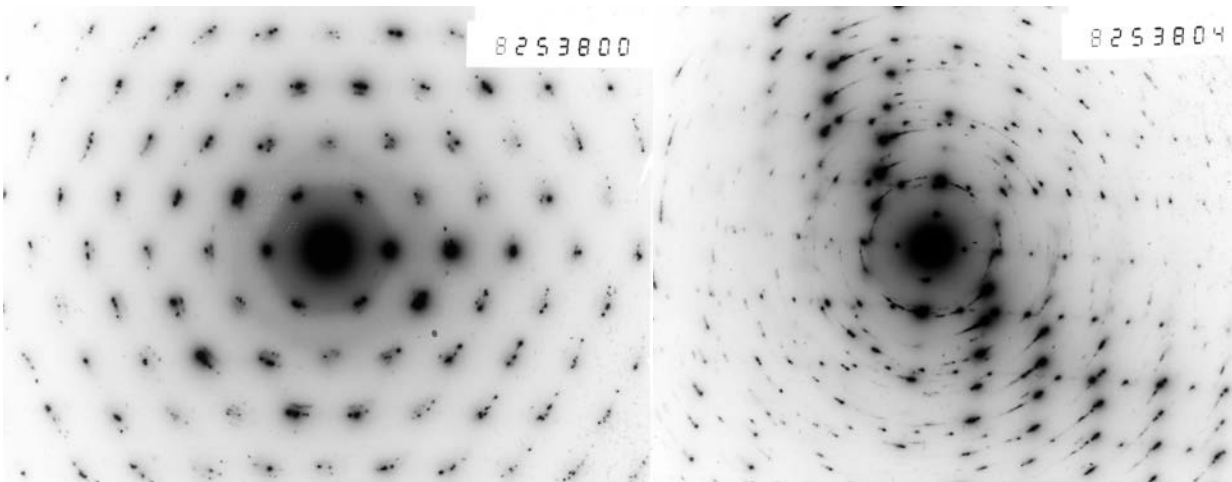
Boundaries of α -phase hasve great many
non-equilibrium dislocations;
Micro-twins are available

Microstructure of alloy E110 (after loading)



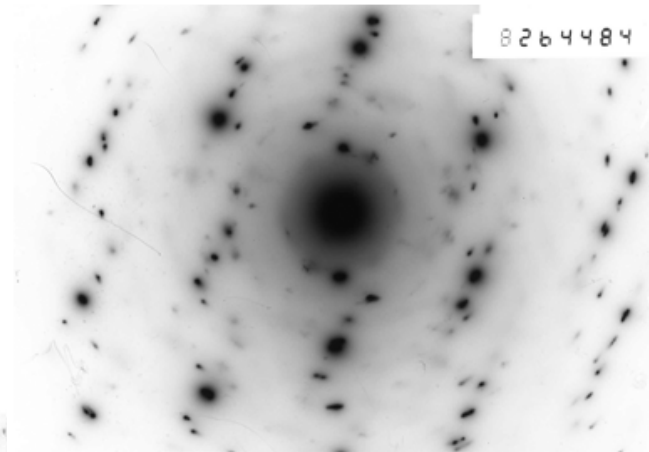
Microelectronic images

$V = 0.21 \text{ km/s}$; $T = 600 \text{ }^{\circ}\text{C}$



Great many dislocation vacancy loops

$V = 0.58 \text{ km/s}$



Parent α -phase continues to exist during pulsed loading. A grain has broken to 3–4 grains having almost similar orientation. However in certain cases, deformation caused parent grains to break into great many small fragments.

Deformation induced misalignment of 5–10° between fragments.

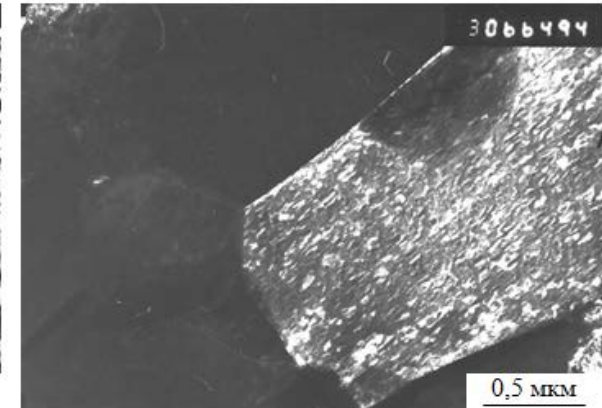
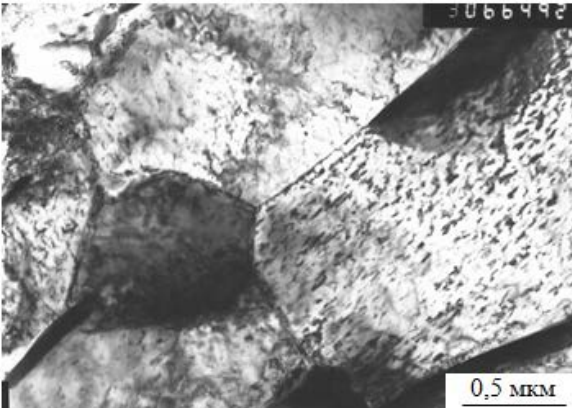
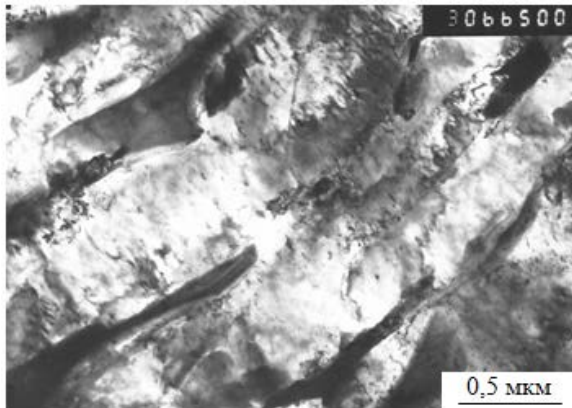
Average grain size of α -phase in alloy was $\sim 1 \mu\text{m}$.

Microstructure of alloy E635 (after loading)

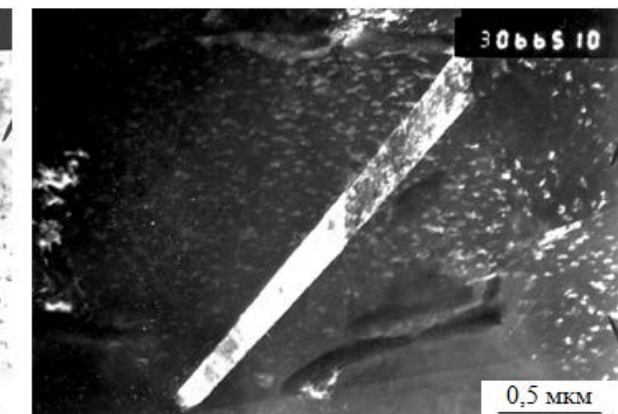
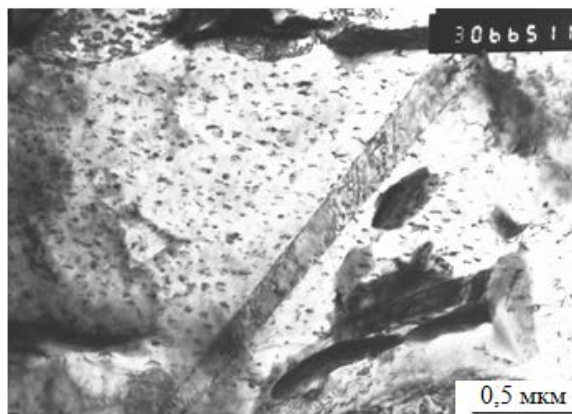
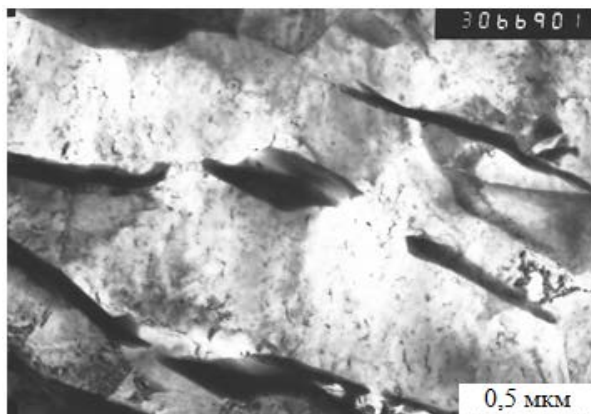


$$V = 0.3 \text{ km/s}$$

Absolutely no deformational micro-twins; many dislocation vacancy loops, this indicates deformation through sliding;
shape of β -phase is recovered



$$V = 0.22 \text{ km/s}; T = 210 \text{ }^{\circ}\text{C}$$

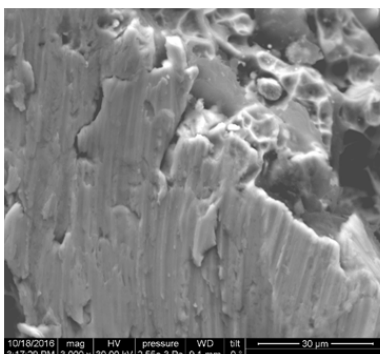
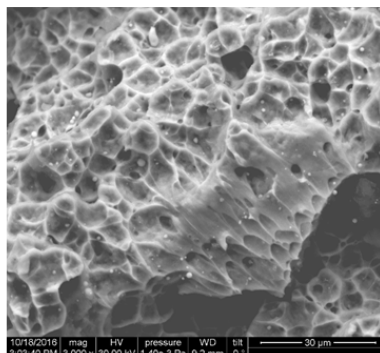
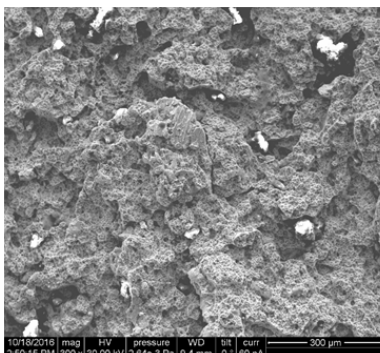
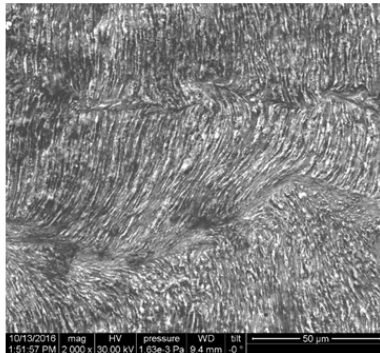
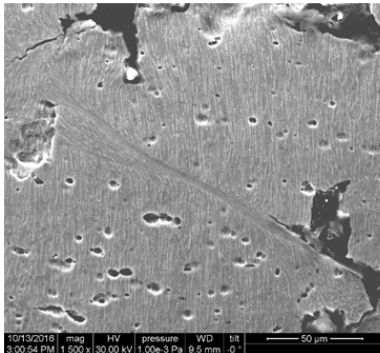


Alloy is observed to have great many dislocation vacancy loops; micro-twins are available just as in the initial state;
grains of β -phase significantly differ;
strong distortion of crystalline lattice

Alloy E125 (Zr-2,5Nb) (after loading)



V = 0.99 km/s



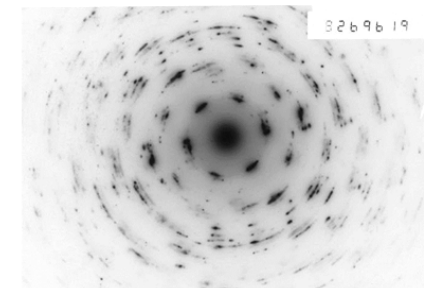
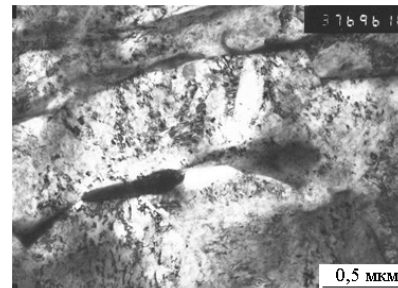
Formation of great many deformation localization bands;
Fracture proceeded in a plastic manner, growth and merging of pores.

V = 0.99 km/s

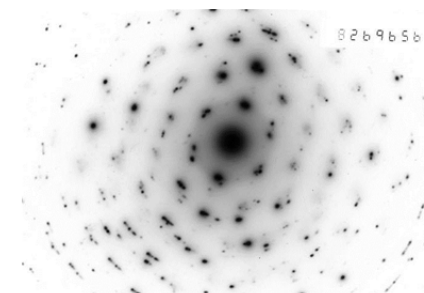
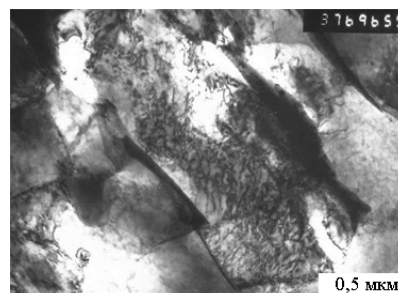
Alloy structure mainly consists of α -phase, amount of recovered ω -phase is less than that in the alloyed zirconium;

deformation through sliding and grain-boundary slipping;

Strong structure refinement due to sliding deformation and $\alpha \leftrightarrow \omega$ transition;



V = 0.3 km/s



Small-sized grains are observed to appear in the structure; plastic deformation through sliding; twinning, individual microtwins

Deformation mechanisms

Zirconium E100

Basic mechanism of deformation is sliding and twinning; role of twins is increasing with the increase of loading intensity;

After high-intensity loading mode ($V = 912 \text{ m/s}$) ω -phase is recovered in zirconium

Zr-1%Nb E110

Basic mechanism of deformation:

at 20°C – sliding and twinning; at 600°C – only sliding;

special feature – plastic flow localization independently on temperature;

E635

Basic mechanism of deformation – sliding and grain-boundary slipping, and also at elevated (up to 210°C) temperature;

high-intensity temperature – only sliding, strong localization of plastic flow and formation of ω -phase;

Zr-2.5%Nb E125

Basic mechanism of deformation:

Plastic deformation through sliding and twinning, individual twins;

high-intensity deformation – through sliding and grain-boundary slipping;

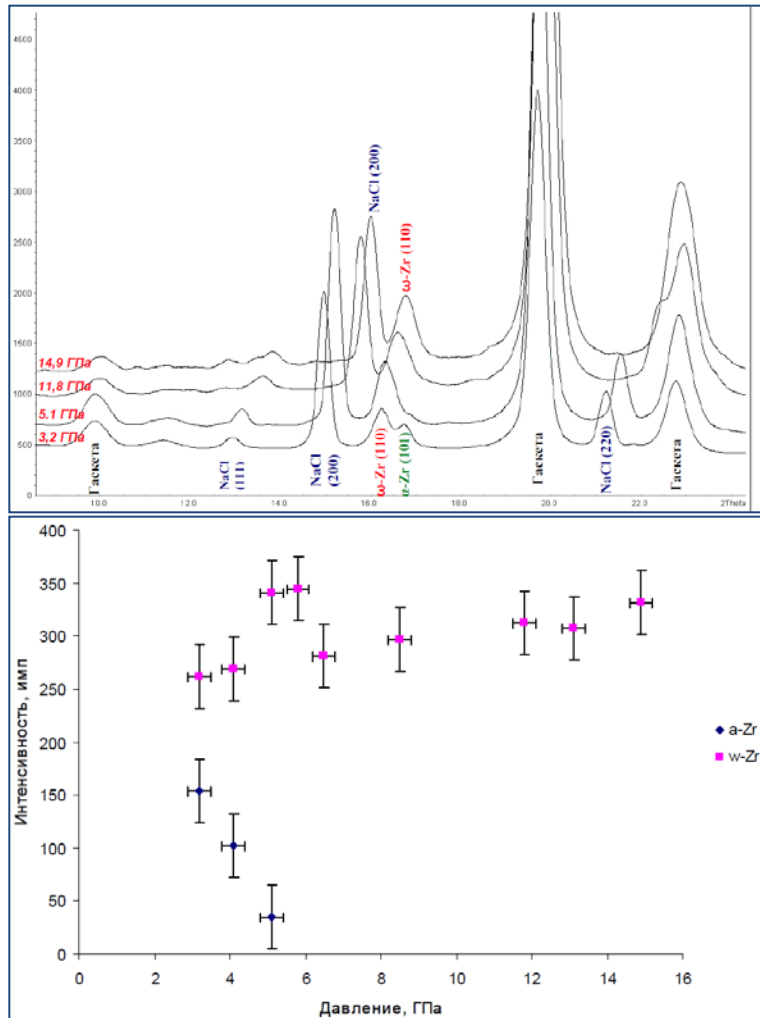
Strong structure refinement due to deformation through sliding and $\alpha \leftrightarrow \omega$ transition

Increase of materials microhardness depends on degree of impact,

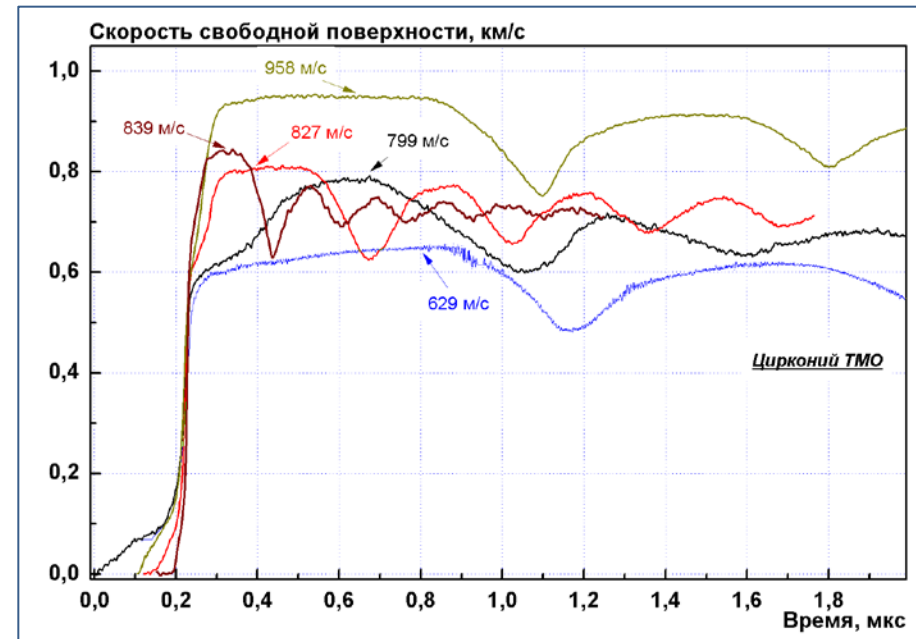
depends on strain-hardening as a result of grain refinement and formation of great many deformation defects – dislocations, subboundaries, and microtwins, as well as formation of high-pressure phase after $\alpha \leftrightarrow \omega$ transition.

Zr $\alpha \rightarrow \omega$ transition

Statics

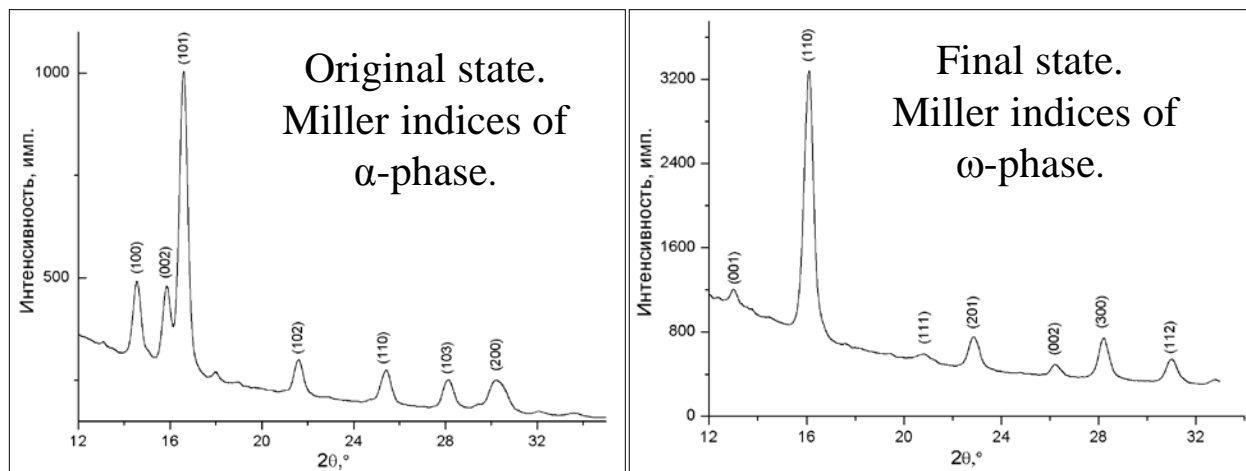
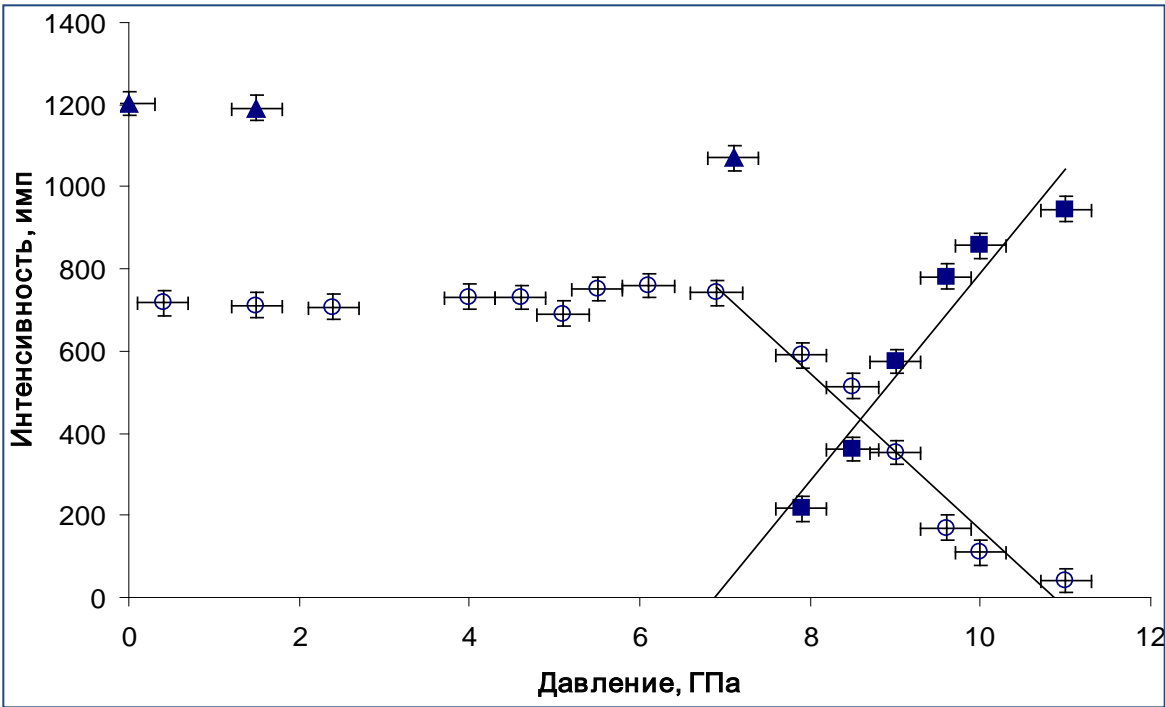


Dynamics



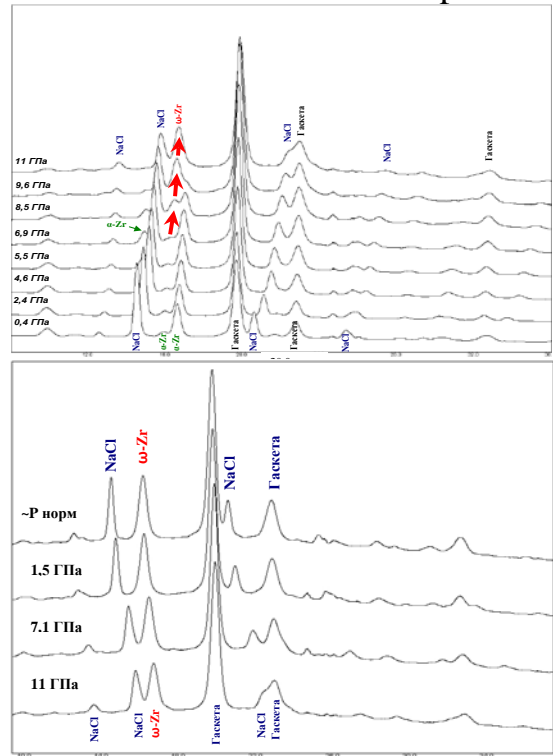
$\alpha \rightarrow \omega$
 0.98 mm - at 8.1 GPa;
 1.99 mm - ~7.7 GPa;
 4 and 6 mm - ~7.4 GPa.

Zr-1%Nb (Э635). $\alpha \rightarrow \omega$ transition



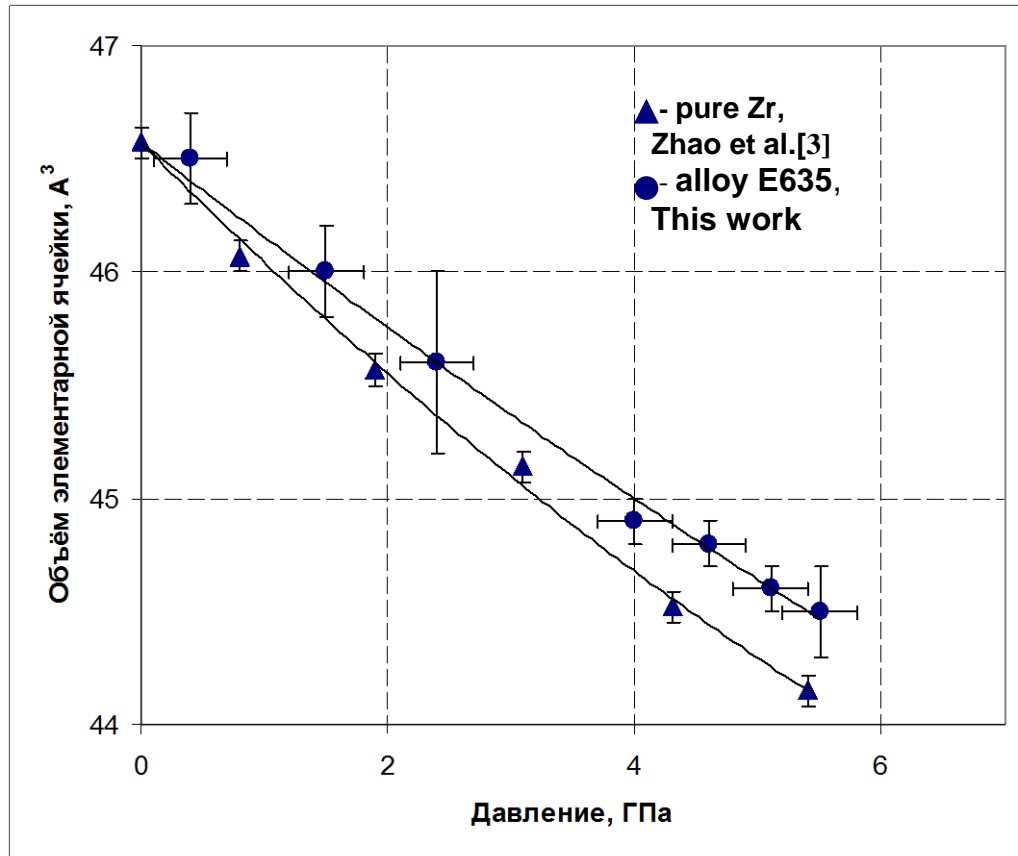
$V_0\omega=23.07\pm0.06\text{\AA}^3$ less volume per one atom in alpha-phase $V_0\alpha=23.29\pm0.04\text{\AA}^3$ at Pnorm.

Loss of volume ~1%. For pure



A.V. Sedov, A.E. Shestakov.
Compressibility and phase transition in zirconium alloy E635 under static loading.
Proceedings of 12th РФМС, 2017.

Zr-1%Nb (Э635). $\alpha \rightarrow \omega$ превращение



Unit cell volume of α -phase in alloy E635 versus pressure (circles). Triangles show experimental data for α -phase of pure zirconium from the work by Zhao et al.[*].

A.V. Sedov, A.E. Shestakov.

Compressibility and phase transition in zirconium alloy E635 under static loading. Proceedings of 12th РФМС, 2017.

Compressibility of α -phase in alloy E635

Estimated isothermal modulus of volume elasticity under normal conditions

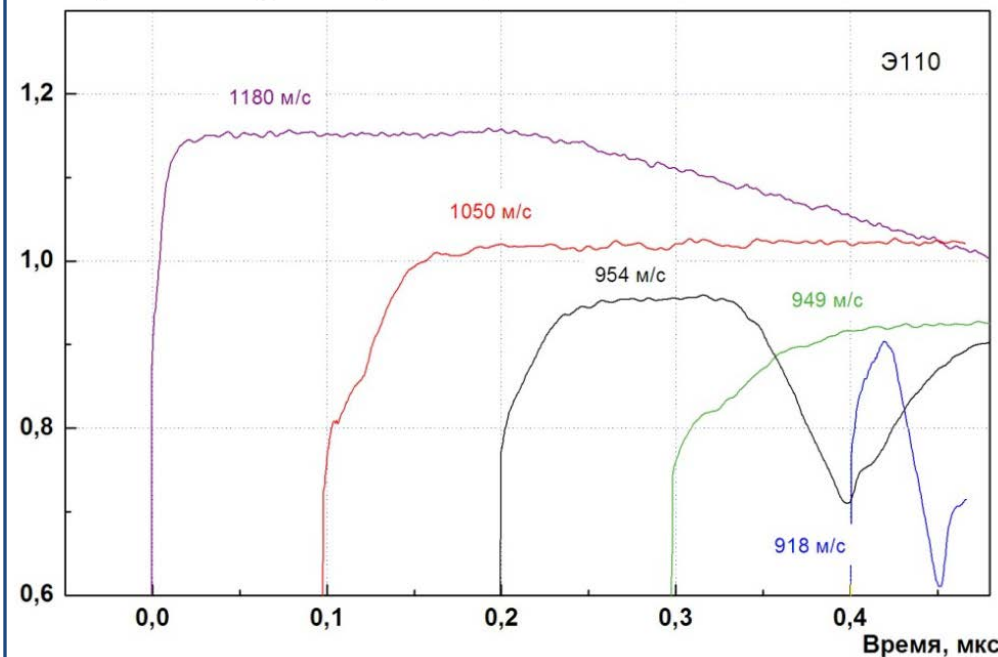
$$K_0^{\text{E635}} \approx 100 \text{ GPa}$$

*. Zhao, Zhang, Pantea, Qian, Daemen, Rigg, Hixson, Greeff, Gray III, Yang, L. Wang, Y. Wang, Uchida. «Thermal Equations of State of the α -, β -, and ω - Phases of Zirconium».

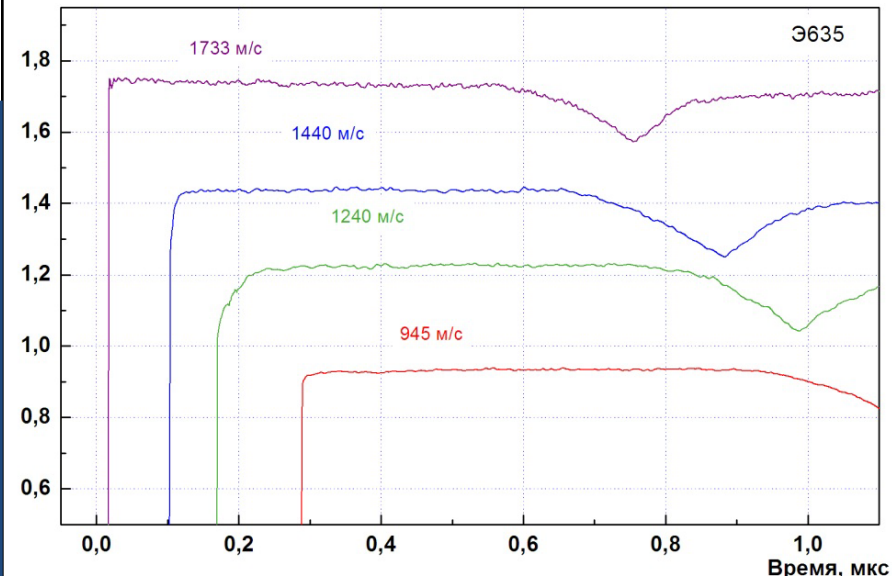
Zr-1%Nb (E110/E635). $\alpha \rightarrow \omega$ transition



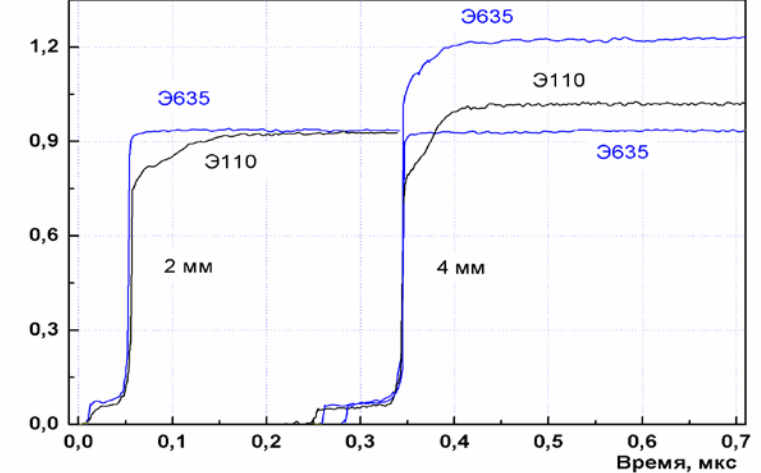
Скорость свободной поверхности, км/с



Скорость свободной поверхности, км/с



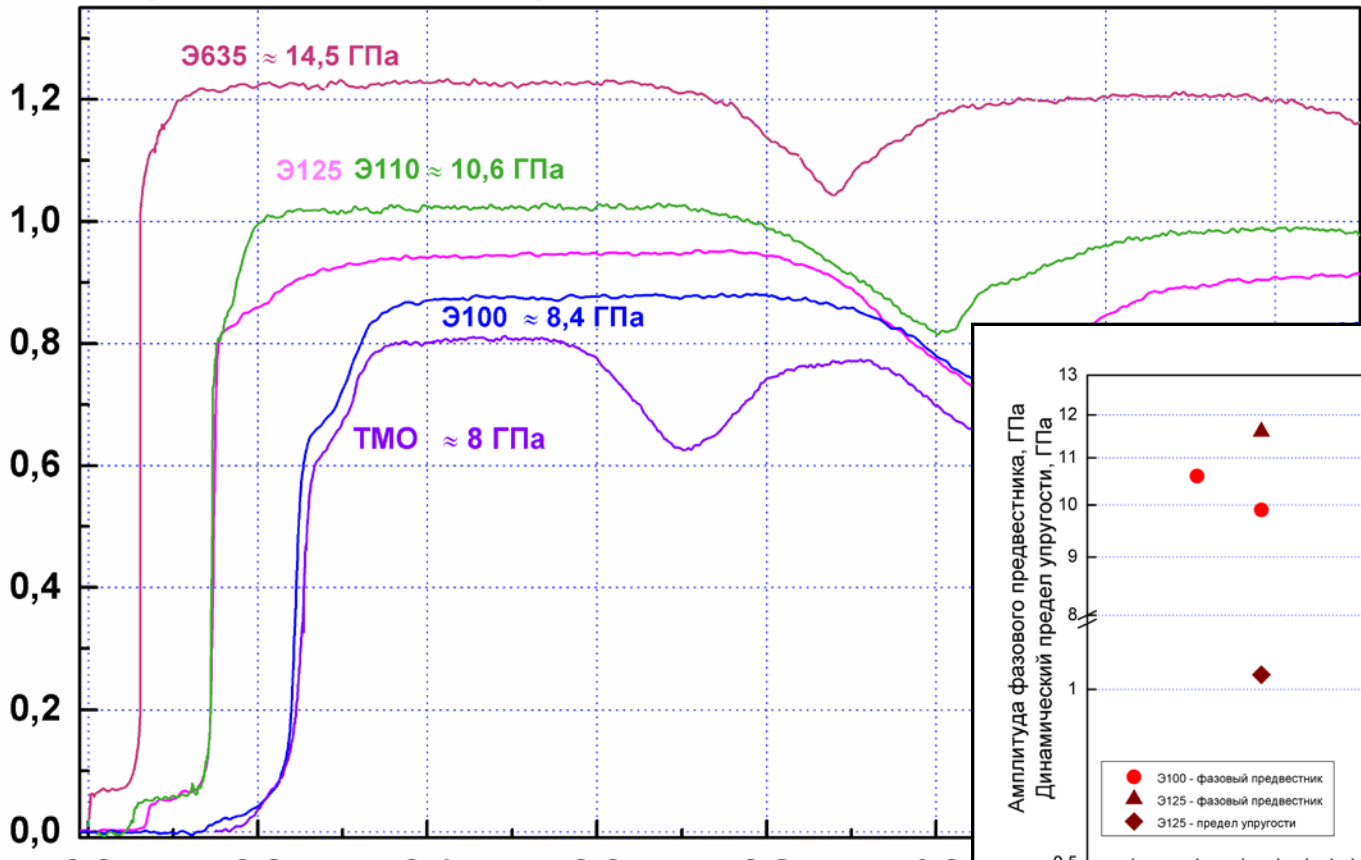
Скорость свободной поверхности, км/с



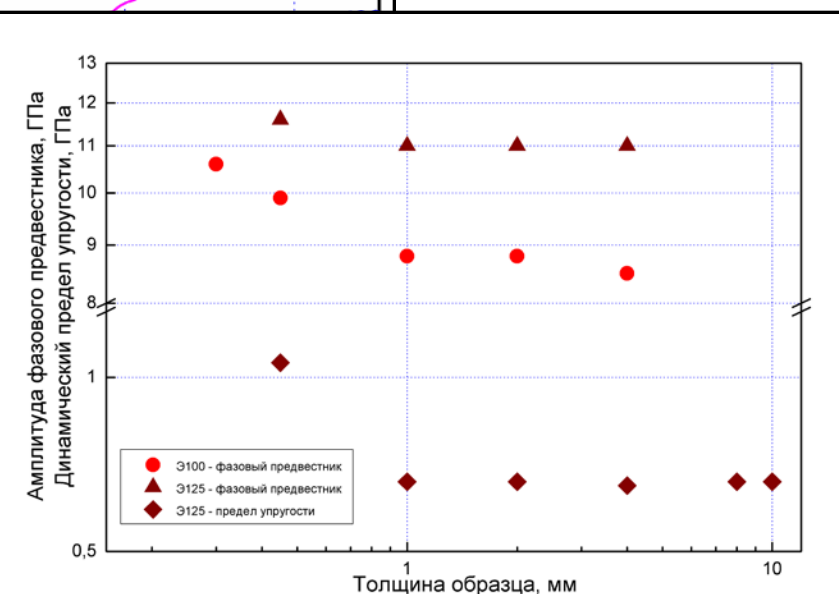
$\alpha \rightarrow \omega$: 0.46 mm - 11.2 GPa; 4 mm - 10.6 GPa.

$\alpha \rightarrow \omega$ transition

Скорость свободной поверхности, км/с

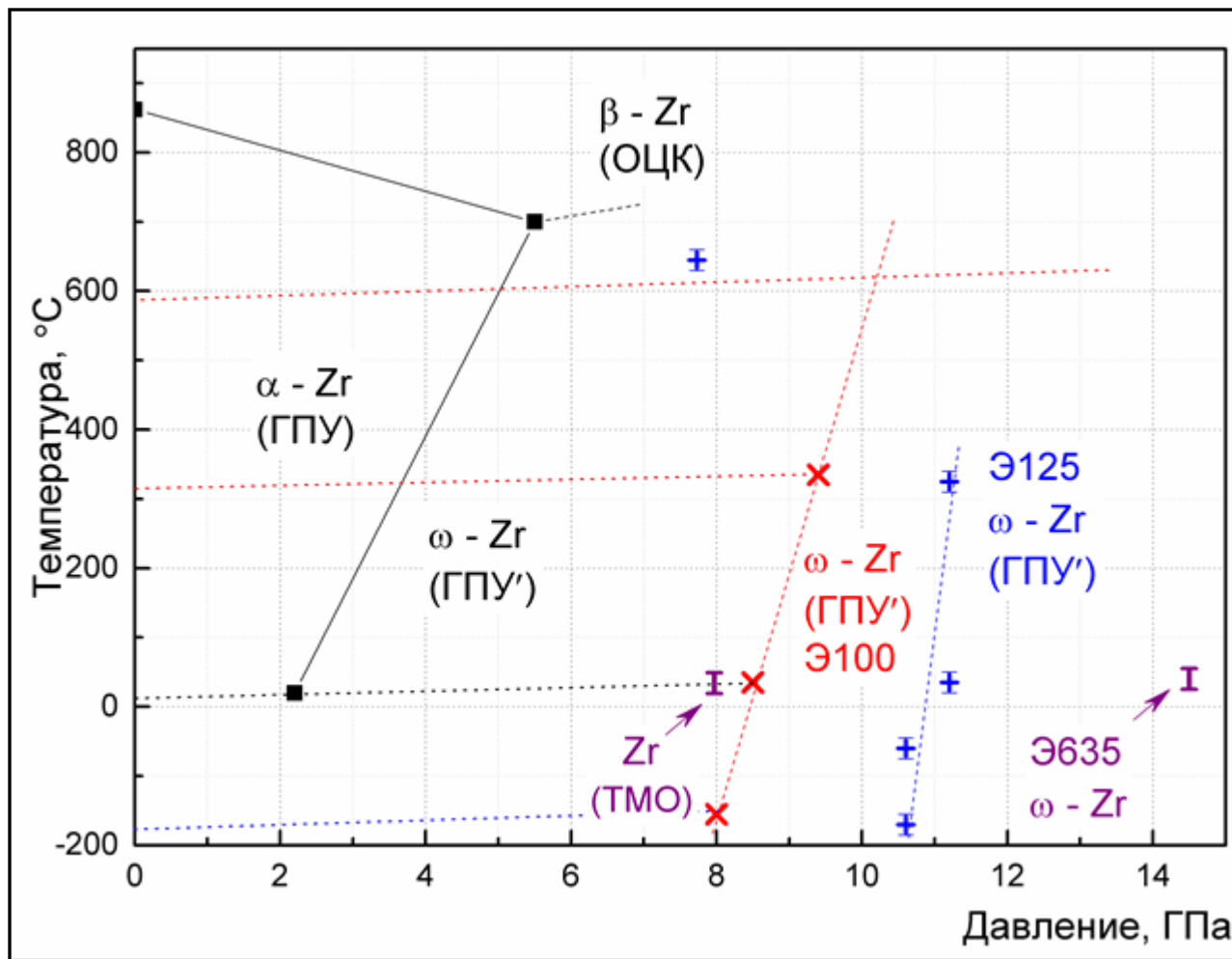


Temperature-, and velocity-dependent dynamic strength of Zr and alloy Zr-2.5%Nb
 S.N. Malyugina, A.V. Pavlenko,
 S.S. Mokrushin, A.S. Mayorova,
 etc. ZNCh-2017



Zr (TMO) $\alpha \rightarrow \omega$: 1 mm - 8.1 GPa; 2 mm - 7.7 GPa; 6 mm - 7.4 GPa. E110 – 8.4 GPa;
 Alloys: E110 $\alpha \rightarrow \omega$: 0.46 mm - 11.2 GPa; 4 mm - 10.6 GPa;
 E635 $\alpha \rightarrow \omega$: 4 mm - 14.5 GPa; E125 $\alpha \rightarrow \omega$: 4 mm - 10.6 GPa.

Temperature dependence of $\alpha \rightarrow \omega$ transition



Conclusion



- Response of samples from E110, E635, and E125 zirconium alloys to shock-wave stimuli is studied within the loading amplitudes from 3 to 26GPa. Shock load duration varied from 0.05 up to 2 μ s.
- Values of dynamic yield stress and dynamic elastic strength are determined in a wide range of strain times (samples thicknesses). Parameters are identified for the empirical relation $\sigma_h = S(h/h_0)^{-\alpha}$ describing relaxation of elastic precursors of zirconium alloys E110 and E635. For E635 alloy $S = 1.158$, $\alpha = 0.148$, for E110 alloy $S = 0.88$, $\alpha = 0.138$.
- Values of spall strength are determined in a wide range of strain rates. Parameters are identified for the empirical relation describing “spall strength versus strain rate”: for E635 alloy - $\sigma_{sp}(E635) = 0.96(V/V)^{0.095}$ and
for E110 alloy - $\sigma_{sp}(E110) = 0.402(V/V)^{0.164}$
for E125 alloy - $\sigma_{sp}(E125) = 1.73(V/V)^{0.057}$
- Strength characteristics of zirconium alloys are measured at elevated temperatures, and namely at ~ 300 , 960 , and $\sim 1000^\circ\text{C}$.
- Spall strength of samples from alloys E635 and E110 heated up to $\sim 300^\circ\text{C}$ remained practically unchanged; dynamic elastic strength increased by 11% and dynamic yield stress decreased by 6%. At the temperature of $\sim 1000^\circ\text{C}$ (material in β -phase), strength loss was noted to be $\sim 20\%$.

Conclusion



- Conditions of equilibrium and dynamic $\alpha \rightarrow \omega$ phase transition are stated; dependences of dynamic behavior of these materials on composition and pulsed loading modes are experimentally determined. Temperature-dependent spall strength of E100 pure zirconium and E125 zirconium alloy are determined.
- For alloys E100 and E125, shock-wave amplitudes that induce $\alpha \rightarrow \omega$ phase transitions are 8.4 GPa and 10.6 GPa, respectively. As a comparison, for zirconium samples subjected to thermomechanical treatment – 7.4 GPa, for alloy E635 – 14.5GPa. Data on temperature-dependent $\alpha \rightarrow \omega$ phase transitions of zirconium and alloy E125 in the range from minus 150 up to plus 600°C are obtained.
- Basic mechanisms of zirconium and its alloys deformation in the range of submicrosecond pressure pulses with the amplitude from 4 to 15 GPa and temperatures from the normal up to 600 °C are determined.
- High strain-rate plastic deformation in test materials can proceed through sliding, twinning, grain-boundary slipping, and plastic flow localization. In addition, much of dissipation of pulsed loading energy in these materials can be induced by $\alpha \leftrightarrow \omega$ phase transition. Mutual dependence is stated to exist between the above deformation mechanisms and intensity, loading conditions, and changes in materials microhardness. Spall fracture in the above materials is stated to proceed primarily according to viscous mechanism through pores growth and merging.

Literature



1. G.P. Kobylyansky, A.E. Novoselov. *Radiation stability of zirconium and alloys on its basis. Reference materials on reactor material science.* Dimirtrovgrad : RF GNTs NIIAR, 1996, p. 176.
2. A.S. Zaimovsky, A.V. Nikulina, N.G. Reshetnikov, *Zirconium alloys and nuclear power engineering.* - M.: Energoatomizdat, 1994.
3. G.I. Kanel, V.E. Fortov, S.V. Razorenov.//Rus.J. UFN ("Uspekhi Fizicheskikh Nauk"- Advances in Physical Sciences), v. 177, № 8, pp. 809-830, (2007).
4. E.N. Avrorin, B.K. Vodolaga, V.A. Simonenko, V.E. Fortov. //UFN, volume 163, No. 5, pp. 1-34.
5. G.I. Kanel, S.V. Razorenov, A.V. Utkin, V.E. Fortov. *Shock-wave phenomena in condensed media.* M.: "Yanus -K", p. 408, (1996).
6. G.I. Kanel. R.J.//Rus.J. PMTF (Applied Mechanics and Technical Physics), v. 42, № 2, c. 1-5, (2001).
7. G.I. Kanel, S.V. Razorenov, A.V. Utkin, V.E. Fortov. *Experimental profiles of shock waves in condensed matter.* M.: FIZMATLIT, (2008).
8. E.B. Zaretsky, G.I. Kanel.//J. Appl. Phys. 110 (7), 073502 (2011)
9. E.B. Zaretsky and G.I. Kanel.// . Appl. Phys. 112, 073504 (2012)
10. E.B. Zaretsky and G.I. Kanel.//J. Appl. Phys. 114, 083511 (2013)
11. E.B. Zaretsky and G.I. Kanel. // Journal of Applied Physics 115, 243502 (2014)
12. *Material physics* : B.A. Kalin, P.A. Platonov, etc. M.: MIFI, 2008, p.672.
13. M.V. Zhernokletov, V.N. Zubarev, R.F. Trunin, V.E. Fortov. *Experimental data on shock compressibility and adiabatic expansion of condensed matter under high energy densities.* Chernogolovka Publisher, (1996).
14. A.V. Pavlenko, S.I. Balabin, O.E. Kozelkov, D.N. Kazakov. // PTE, No. 4, pp. 122-124, (2013).
15. A.V. Pavlenko, S.N. Malyugina, V.V. Poreshitov, I.N. Lisitsyna. // PTE, No.2. pp. 127-129, (2013).
16. S.S. Mokrushin, N.B. Anikin, S.N. Malyugina, A.A. Tyaktev, A.V. Pavlenko. // PTE, No.4, pp.107-110, (2014).
17. G.V. Garkushin, G.I. Kanel, S.V. Razorenov. // Solid state physics, 2012. V. 54, No. 5. pp. 1012-1018.
18. D.N. Kazakov, A.S. Mayorova, A.V. Pavlenko, S.N. Malyugina, etc. MTT, No.6, pp. 77, 2014

Thank you for attention!!!